

Life Cycle of Major Sudden Stratospheric Warmings in the Southern Hemisphere from a Multimillennial GCM Simulation

MARTIN JUCKER^a AND THOMAS REICHLER^b

^a *Climate Change Research Centre and ARC Centre of Excellence for Climate Extremes, University of New South Wales, Sydney, New South Wales, Australia*

^b *Department of Atmospheric Sciences, University of Utah, Salt Lake City, Utah*

(Manuscript received 7 June 2022, in final form 14 September 2022)

ABSTRACT: Sudden stratospheric warmings (SSWs) are rare in the Southern Hemisphere (SH), making it difficult to study possible precursors or subsequent impacts. Using a multimillennial coupled climate model simulation producing 161 SSWs in the SH, we present a detailed study of their life cycle. We show that SH SSWs are predominantly displacement events forced by wave-1 planetary waves, and that a surface signature similar to the negative phase of the Southern Annular Mode (SAM) is detectable up to two months before the onset date, but there is a tendency for a transition from wave 1 before to zonally symmetric anomalies after onset. We identify a strong weakening of the Amundsen Sea low as one of the most prominent precursors, which weakens the climatological wave-2 and wave-3 stationary waves and strengthens wave-1 forcing. Compared to their northern counterparts, SH SSWs generally have a longer time scale, and while there is evidence of pre-onset forcing related to tropical sea surface temperatures, the Indian Ocean dipole is more important than El Niño–Southern Oscillation.

SIGNIFICANCE STATEMENT: Sudden stratospheric warmings (SSWs) are extreme events where the winter polar stratosphere warms within a few days to temperatures usually only experienced in summer. These events are rare in the Southern Hemisphere. Therefore, both the observational record and standard climate model simulations are not enough to understand how SSWs develop, or how they might change surface weather. Here we use very long global climate simulations that produce a large number of SSWs in the Southern Hemisphere to study the development and impact of these events. This includes possible precursors as well as the influence they have on surface weather after they occur.

KEYWORDS: Dynamics; Stratosphere-troposphere coupling; Stratosphere; Climate variability

1. Introduction

Sudden stratospheric warmings (SSWs) are extreme events in the winter polar stratosphere, during which the usually strong polar night jet (or polar vortex) strongly decelerates or even reverses direction (Butler et al. 2015). While the exact number of events depends on the details of their definition, SSWs are extremely rare in the Southern Hemisphere (SH) and are confined to early to late spring (Jucker et al. 2021). However, when they do occur, events such as observed in 2002 and 2019 have been linked to extended periods of unusual weather over the SH, in particular during the following summer (Thompson et al. 2005; Lim et al. 2021a), but also during spring (Jucker and Goyal 2022). Due to their rareness, it is impossible to study the life cycle of SSWs in the SH from observational datasets, reanalyses, or even CMIP5/6 (Jucker et al. 2021).

One way of increasing the number of events and therefore statistical significance is to extend the analysis to include events that do not satisfy traditional SSW definitions from the Northern Hemisphere (NH) but that still show similar behavior and surface impact at least in the sense of an ensemble

mean. Examples include the studies by Thompson et al. (2005), who analyzed the seven most extreme events prior to 2002 in terms of the Southern Annular Mode (SAM) index at 10 hPa, and found similarities between those and the major SSW of 2002. Similarly, Wang et al. (2021) composited the evolution of multiple variables from October to February for the 10 most extreme years as defined by anomalies of polar-cap averaged geopotential height at 50 hPa, and found that the Amundsen Sea low (ASL) was anomalously weak in the spring, and sea ice anomalies were consistent with the accompanying anomalous surface winds. Furthermore, Byrne and Shepherd (2018) and Lim et al. (2018) found that early polar vortex breakdowns resulted in summer circulation anomalies that were similar to those expected after an SSW.

Here we will keep our focus on major SSWs [where the zonal mean zonal wind at 10 hPa and 60°S becomes easterly (Charlton et al. 2007); hereafter simply referred to as SSWs] and get around the problem of low number of events by using a unique near-10 000-yr coupled climate model simulation, which is identical to the present-day simulation of Jucker et al. (2021). We note that technically this excludes events like the vortex weakening of 2019 that did not quite reach the criterion of zero zonal mean zonal wind at 10 hPa and 60°S. This simulation produces 161 major SSWs, which allows for meaningful statistical analysis of the life cycle of SSWs in the SH.

Corresponding author: Martin Jucker, publications@martinjucker.com

We will show that many of the tropospheric changes found after the SSWs (usually referred to as “impact”) are already present long before the onset date of the SSW, and that in particular over Australia these pre-existing anomalies become stronger after the onset date, whereas in the Amundsen Sea the anomalies become significantly weaker after onset.

In section 2 we will introduce the data, SSW definition, and methods for our study, before analyzing the components of the SSW life cycle near the surface (section 3), at the interface between the troposphere and in the stratosphere (section 4), and the stratosphere alone (section 5). We summarize our findings in section 6.

2. Data and methods

We will analyze daily data from a 9990-yr coupled climate model simulation, which was used previously for studies by Horan and Reichler (2017), Jucker and Reichler (2018), Jucker et al. (2021), and Reichler and Jucker (2022). The model is a high-top version of GFDL’s CM2.1 with 48 vertical levels in the atmosphere and it has been shown to simulate stratospheric dynamics and stratosphere–troposphere coupling very well (see above literature for details on model validation), and it also produces a realistic El Niño–Southern Oscillation (ENSO) (Wittenberg et al. 2006) and ocean circulation, in particular in the Southern Hemisphere (Gnanadesikan et al. 2006). In appendix B, we have performed additional model evaluation to assess the reproduction of the Southern Annular Mode pattern and its relation to other surface variables, the representation of stationary waves, and ENSO-related teleconnections.

Given the luxury of a large number of events in the model simulation, we focus entirely on the classic definition of major SSWs following Charlton et al. (2007); that is, an SSW is defined as a complete reversal of the zonal mean zonal wind at 60°S and 10 hPa (henceforth u_{1060}), followed by a recovery to westerly u_{1060} before the seasonal breakdown of the polar vortex in spring (also known as the “final warming”). We also require that the onset date is at least 20 days before the final warming, and two events would be counted as the same if they occurred within 20 days of each other, although this never happened in the Southern Hemisphere (neither in observations nor our model simulation). The onset date is defined as the first day the zonal mean zonal wind becomes easterly, and there are 161 SSWs in our simulation.

Different variables and derived quantities are introduced when appropriate. We use lagged composites as our main analysis tool, and whenever we refer to “anomalies” we mean daily anomalies with respect to the daily seasonal cycle from the full simulation. SSW evolution is split into an early stage (from 60 to 20 days before onset), a mature stage (from 20 days before to 20 days after onset), and a late stage (from 20 to 60 days after onset). This is similar to studies of the life cycle of SSWs in the Northern Hemisphere (e.g., Limpasuvan et al. 2004). When analyzing composites over all SSWs, we assess statistical significance with a two-tailed t test against the null hypothesis of zero anomalies, and anomalies which are not significant at the $p = 5\%$ level are hatched in all figures.

In many sections in this paper we compare the SSW life cycle to climatology. However, given that most SSWs occur in late spring (Jucker et al. 2021), the life cycle inevitably includes an effect of seasonal cycle, even if we only analyze anomalies with respect to the day of year climatologies. For instance, the variability of many variables is larger in late spring than early spring or even winter, meaning that comparisons between the early and late stages of the SSW life cycle to climatology—or years without SSWs—have to take into account the uneven seasonal distribution of SSWs.

To do this, we define a random set of years without SSWs, which is 10 times larger than the set of SSW years; that is, we use 1610 randomly selected years from the 9990-yr simulation, with the two conditions that no year may be sampled twice, and no year may include an SSW. This task is very resource intensive, which is why we are using 1610 years rather than all non-SSW years from the simulation. Then, for each of the 161 SSW onset dates, we randomly choose 10 non-SSW years, but use the same day of the year. For instance, if an SSW occurs on 24 September in year 51, we sample ten 24 Septembers of non-SSW years. Then, we construct a similar “life cycle” as for actual SSWs (i.e., we retain the time period from 60 days before to 60 days after 24 September of each of the 10 non-SSW years). After doing this for every SSW, we then have a set of 1610 random “events” without SSW, but with the same seasonal distribution as the 161 SSWs. We call this the “climatology.”

3. Surface evolution

As most interest in SSWs is in their surface impact, we will start in the troposphere and work our way up to the stratosphere in later sections. As described in section 2, we will analyze different aspects of the life cycle of major SSWs in the SH by means of event composites, grouped into the early, mature, and late stages of the evolution. We will start with the evolution of sea level pressure, surface temperature, and precipitation in Fig. 1.

a. Sea level pressure

The sea level pressure (SLP) has a strong wave-1 component in the early stage (Fig. 1a) but becomes more zonally symmetric with lag to become annular at the late stage (Fig. 1c). During the early stage, midlatitude SLP anomalies are mainly negative except over the Atlantic basin, where they are positive, and there is a peak negative signal 180° farther west over the Tasman Sea, confirming the strong wave-1 component in midlatitudes (Fig. 1a). There are also positive SLP anomalies close to South America, which are associated with a strong positive signal in the region of the Amundsen Sea low during the early stage. The ASL anomaly is very distinctive even though at high latitudes, SLP anomalies are positive everywhere. During the mature stage, although the SLP anomalies are more annular, there is now a wave-3 signal in the band of negative anomalies over the Southern Ocean, with local minima in the Atlantic, the Indian Ocean, and south of New Zealand (Fig. 1b). During the late stage (Fig. 1c), SLP anomalies are again more zonally symmetric,

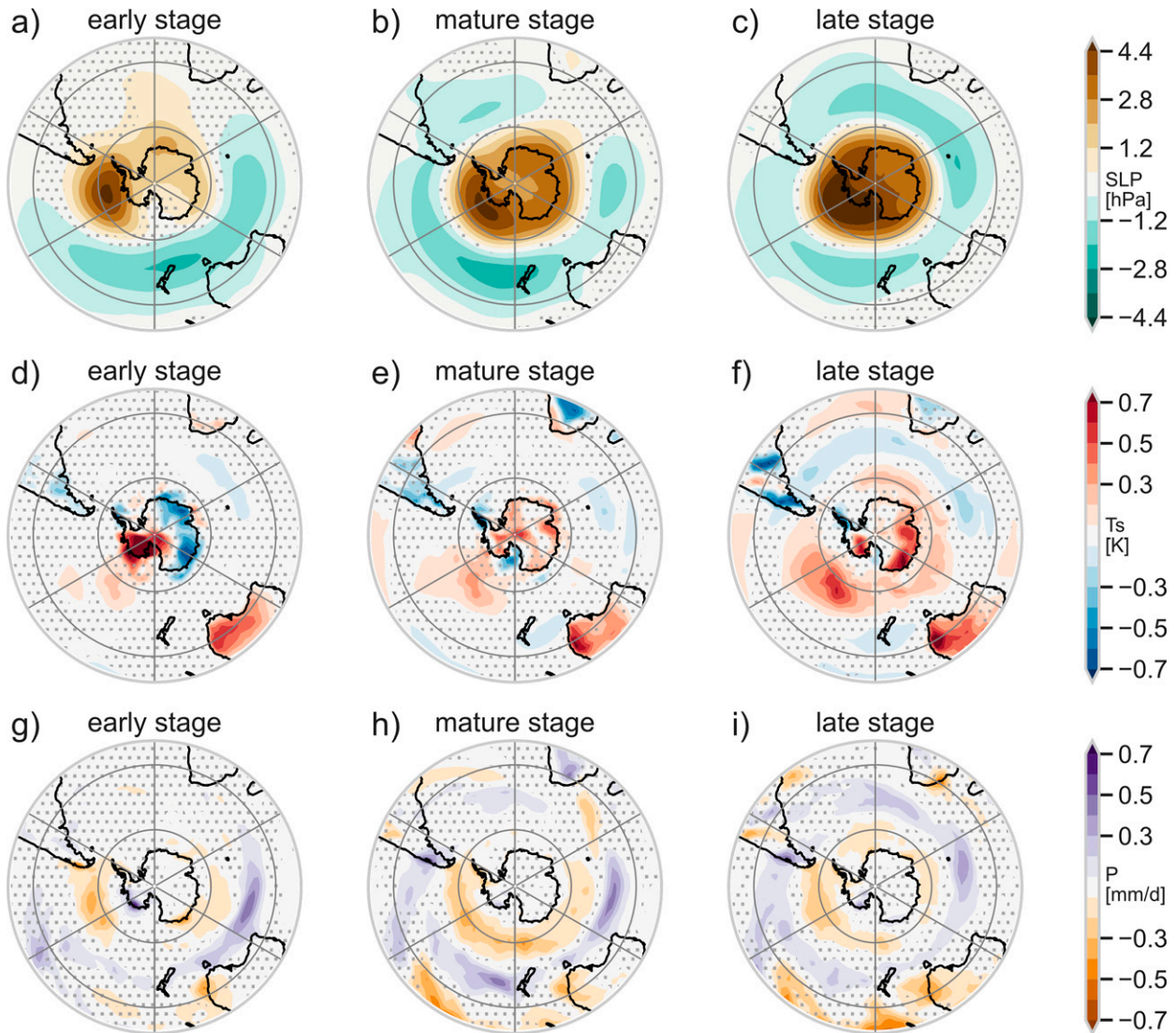


FIG. 1. Surface impact as measured by (a)–(c) sea level pressure, (d)–(f) surface temperature, and (g)–(i) precipitation, grouped into three 40-day lag periods (panel titles) corresponding to (left) early, (center) mature, and (right) late stages. For all variables, the hatching denotes regions where the anomalies are not significantly different from zero based on a two-tailed *t* test at the 95% level.

with the early stage wave-3 pattern replaced by weak and unequally spaced maxima over the Southern Ocean, and an almost circular positive anomaly over the Antarctic continent. Equatorward of the Southern Ocean, SLP anomalies are statistically significant only in the Pacific and Atlantic basins. Over land, there is only a small area of significant SLP anomalies over Chile at the late stage, whereas during the early and mature stages larger sections of Australia, South Africa, and South America also show significant anomalies.

The strong wave-1 component of the early stage SLP anomalies is related to an anomalously weak ASL and is consistent with earlier findings from reanalysis (Wang et al. 2021). It can be seen as an important precursor for SSWs, as the longest waves most easily travel into the stratosphere (Charney

and Drazin 1961). We will show in section 4 that the stratospheric wave forcing is dominated by wave 1 (Fig. 8), and previous literature has also stressed the importance of that wavenumber in SH SSWs (Newman and Nash 2005; Shen et al. 2020; Rao et al. 2020; Kwon et al. 2020; Lim et al. 2021a).

However, it is not obvious how the *weakening* of the ASL can cause an *increase* in wave-1 forcing, and therefore we analyze the high-latitude SLP anomaly during the early stage in more detail in Fig. 2. Figure 2a shows early stage climatological SLP stationary waves (blue, solid; defined as climatology minus zonal mean), SSW anomalies (orange, dashed), and the sum of climatology plus anomalies (green, dotted). Figure 2b shows the Fourier decomposition of SLP into wavenumbers, with the same color coding and line styles (or hatching). We

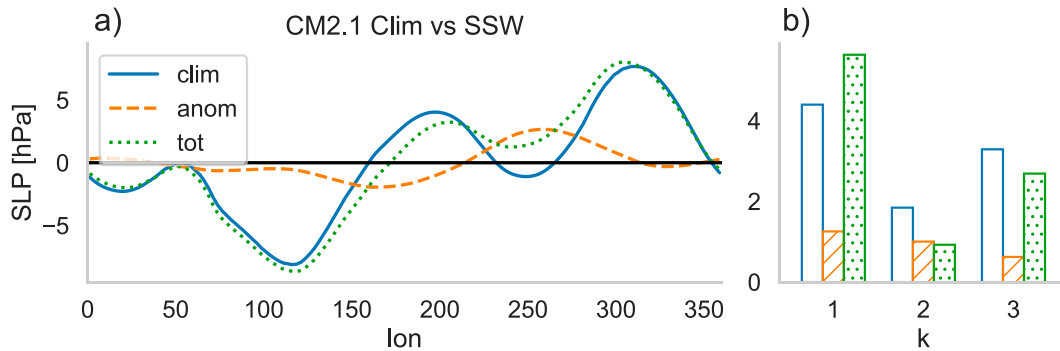


FIG. 2. (a) Zonally asymmetric sea level pressure (SLP) averaged between 70° and 50°S for (blue) August–September climatology, (orange, dashed) early stage SSW anomaly, and (green, dotted) climatology plus anomaly. (b) Leading Fourier amplitudes (wavenumbers 1–3) for the same quantities. The strong SLP anomaly visible in Fig. 1a related to the Amundsen Sea low (ASL) is located around 250°E, and corresponds to a weakening of the climatological low, which strengthens the global wavenumber-1 forcing.

refer the reader to [appendix B](#) for a general evaluation of the reproduction of stationary waves in our model compared to ERA5.

From Fig. 2a it is evident that the strongest SLP anomaly is positive and coincides with the location of the climatological low around 250°E, meaning that the anomaly results in a weaker ASL compared to climatology. The location and zonal extent of the climatological ASL is such that it weakens the total wave-1 component in favor of a wave-3 component [cf. blue bars in Fig. 2b]. In contrast, the spectrum and relative phase of the SLP anomaly associated with the early stage of the SSW life cycle result in a stronger wave-1 component at the expense of both wave-2 and wave-3 components (cf. blue bars to green dotted bars). Therefore, the overall strength of the wave-1 component increases thanks to an “ironing out” of the climatological wave-3 component, which is in turn due to a weakening of the ASL.

b. Surface temperature and precipitation

Even if SLP anomalies have a strong wave-1 component in the early stage, they still project onto the negative phase of the Southern Annular Mode at all stages, and much of the surface temperature and precipitation anomalies are consistent with what we would expect from a negative SAM (see [appendix B](#)). This includes warmer and drier than usual Australia (mostly in the east and south) and colder and wetter than usual southern South America ([Gillett et al. 2006](#)). However, linked to the positive SLP anomalies over the Atlantic, the early stage surface temperature anomalies over South Africa are slightly positive, opposite to the canonical negative SAM signals (Fig. 1d). These anomalies are not statistically significant during the early stage, and switch sign during the mature stage, when they also become significant. Similarly, there is an insignificant cold anomaly over South America coinciding with a (significant) positive anomaly over the South Pacific during the early stage associated with the weaker ASL. These anomalies become stronger and are accompanied by significant precipitation anomalies during the mature stage (Figs. 1e,h). Over Antarctica, a similar picture emerges, where

in the early stage East Antarctica is cooler and West Antarctica warmer than usual (Figs. 1d,g), whereas positive temperature anomalies prevail over the entire Antarctic continent (except the peninsula) during the mature and late stages (Figs. 1e,f).

An important result to stress here is that over Australia and South America, the temperature and precipitation anomalies are already present two months before the onset of the SSW, and persist throughout the SSW life cycle. This is similar to [Lehtonen and Karpechko \(2016\)](#), who found that in the Northern Hemisphere, cold anomalies are often present already before the onset of SSWs and can be seen as a direct consequence of SSW precursors. However, similar to [Garfinkel et al. \(2017\)](#), who found that such pre-existing anomalies can become even more extreme after the onset of SSWs in the NH, we find that in the SH SSWs still have a measurable effect at the surface at positive lags. In particular, the main impact of the SSWs seems to be to make the pre-existing anomalies more zonally symmetric at positive lags. Surface temperature anomalies in the early stage can largely be explained from the SLP anomalies via geostrophic wind balance, as the pressure anomaly over the Amundsen Sea enforces northerly (and therefore onshore) winds over the region of strong warming in the Antarctic Peninsula, and southerly winds over southern South America, thus cooling that region. The anomalously low surface pressure just south of Australia brings anomalous westerly winds over that continent, resulting in increased advection of hot and dry air from the interior deserts toward the East Coast.

To shed more light onto the persistence of these early precursors, we next analyze probability distribution functions (PDFs) of precipitation (Fig. 3) and surface temperature (Fig. 4), both of which are standardized anomalies by day of year and averaged over the selected regions of southern Africa (SAF), western Australia (WAUS), eastern Australia (EAUS), New Zealand (NZ), southern South America (SSA), Indian sector Antarctica (IA), and Pacific sector Antarctica (PA). The PDFs are roughly centered over the relevant regions (refer to [appendix A](#) for their exact definitions).

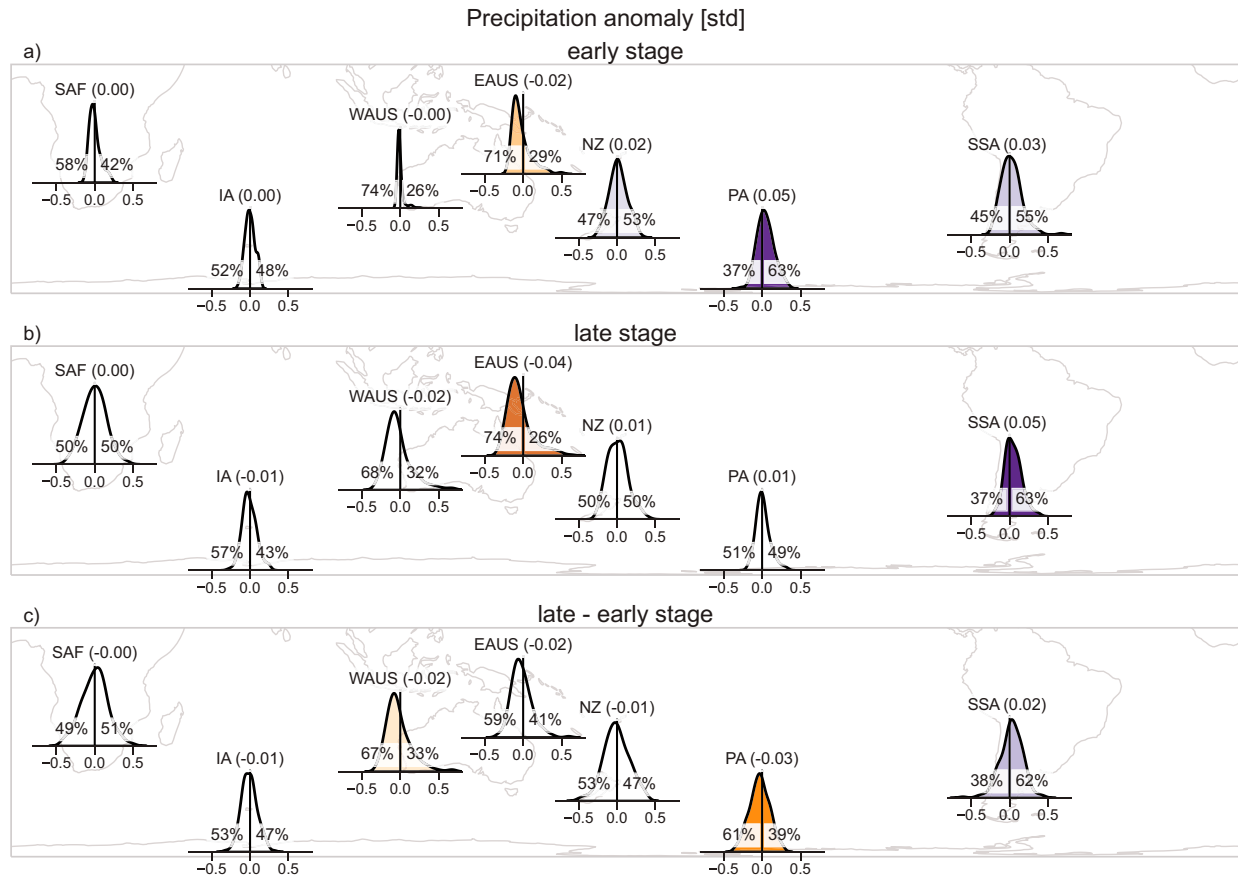


FIG. 3. PDFs for (a) early stage and (b) late stage standardized precipitation anomalies for different regions in the Southern Hemisphere. (c) PDFs of precipitation change between the late and early stages. The x axis is labeled in units of standard deviation (by day of year), and the percentages show the fraction of events with positive or negative values. Numbers in the title show the means. Color is according to mean value, with brown/orange drier and blue wetter than usual. Color is made transparent linearly with p value from a Kolmogorov–Smirnov test if the actual distribution is distinct from a distribution sampled from 1610 non-SSW years (i.e., PDFs with associated p values of more than 10% are not filled). The distributions were estimated using a kernel density estimate (KDE). See appendix A for the definitions of each region and significance testing.

Figures 3a and 4a show the anomaly PDFs during the early stage, Figs. 3b and 4b those during the late stage, and Figs. 3c and 4c the differences between the late and early stages. The PDFs are constructed by averaging each event spatially and temporally over the predefined regions and lags for each relevant stage within the life cycle, and then producing PDFs across all detected events. The percentages indicate the fraction of events with positive (right side) or negative (left side) values. The means for each PDF are reported in the parentheses of the title, and coloring corresponds to the mean value. Significance is tested against our ensemble of 1610 events from years without SSWs as described in section 2. Shading of the PDFs is made transparent depending on the p value of each PDF from a two-sided Kolmogorov–Smirnov test: fully opaque for $p = 0$, and linearly decreasing to fully transparent (no shading) for $p > 10\%$. We note that the standardization of precipitation has the effect that the anomalies seem small with respect to the climatological standard deviation (as evidenced by the values along the x axis for each region), but

this is more due to the fact that precipitation is positive definite than the rainfall anomalies being small. We invite the reader to compare the PDFs of Figs. 3 and 4 with the climatological PDFs of Figs. A2 and A3 in appendix A. There is a strong seasonal cycle in both the mean and variability of precipitation and surface temperature, and standardizing allows to remove the effect of increased variability in late spring in the analysis.

As expected from the composites of Fig. 1, precipitation anomalies are significantly negative over eastern Australia both during the early and late stages (Fig. 3). There is a small decrease in mean precipitation between the early and the late stages, but the change is not significant at the 90% level (no shading over EAUS in Fig. 3c). This confirms our previous observation that in EAUS, the precipitation anomalies usually attributed to SSWs are already present before onset. About two-thirds to three-quarters of all SSWs show a negative precipitation anomaly in that region throughout the SSW life cycle. While western Australia's precipitation anomalies

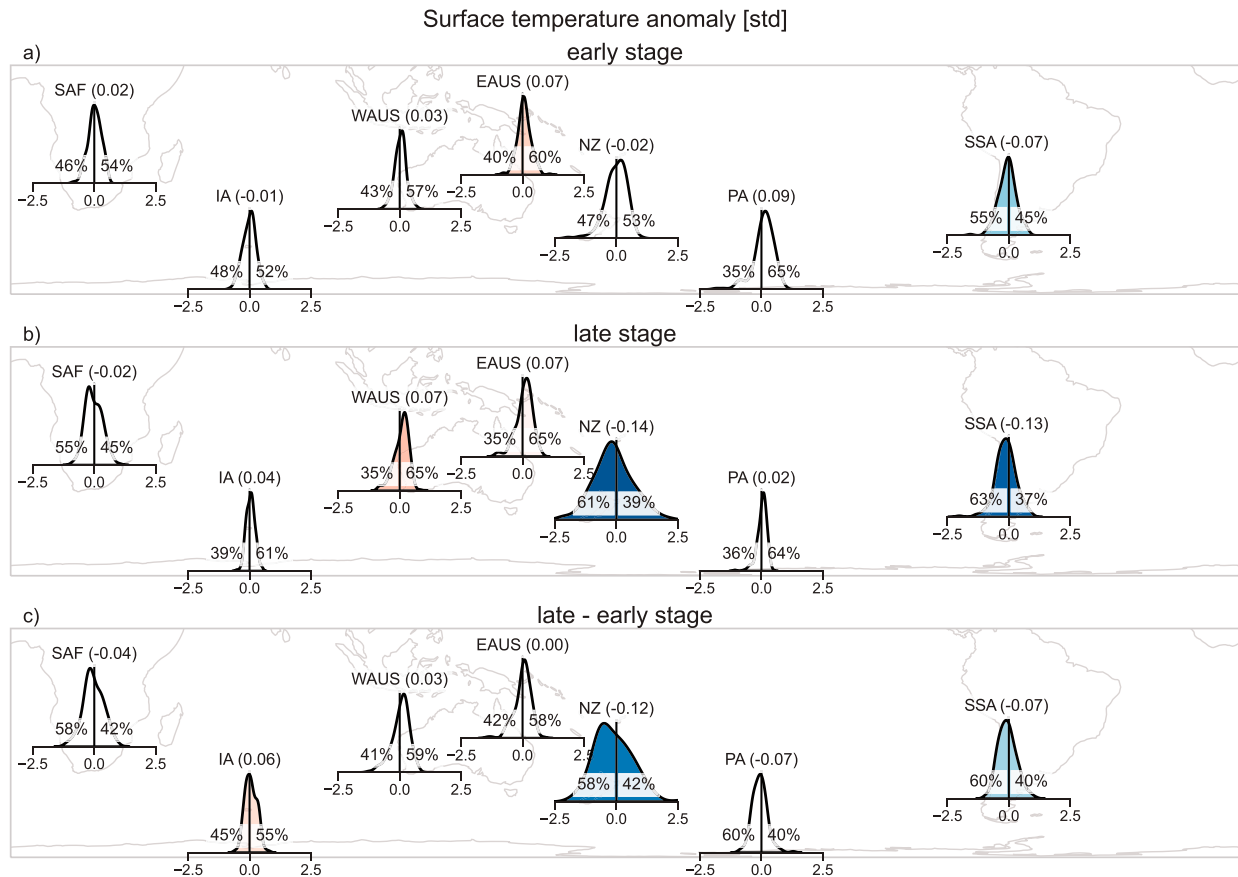


FIG. 4. As in Fig. 3, but for standardized surface temperature anomalies. Red means warmer and blue cooler than usual on average.

are not significant for both the early and late stages, there is a significant change toward less precipitation between the two stages, with two-thirds of the events showing a decrease. The only other regions with significant precipitation changes between the late and early stages are southern South America, which starts with slightly more precipitation at the early stage and becomes even wetter at the late stage, and the Pacific sector of Antarctica, which changes from significantly wetter during the early stage to neutral during the late stage. This region (PA) is also the only region in which the changes between the early and late stages are of opposite sign to the anomalies during the early stage, which we attribute to the localized ASL response discussed around Fig. 1, and which suggests that this region is an important precursor of SSWs.

As with precipitation, the surface temperature anomaly PDFs (Fig. 4) show that both Australian regions have more extreme warm days during the late stage with a positive shift in the mean, but the changes between early and late stage are not significant. The only regions with significant shifts between early and late stages are over Antarctica in the Indian sector (IA) with a slight warming, and over New Zealand and southern South America, which both experience colder temperatures during the late stage. Whereas southern South America already has a negative mean temperature anomaly

during the early stage, which then about doubles during the late stage, New Zealand shifts from a neutral PDF during the early stage to a strongly negative mean temperature anomaly during the late stage. However, note that although the shift toward colder temperatures over New Zealand is significant, only 61% of all events actually show negative anomalies.

c. Tropical sea surface temperatures

In addition to two-dimensional variables we also analyze ENSO and Indian Ocean dipole (IOD) indices, referring to the main modes of tropical sea surface temperature (SST) variability. From the different ENSO indices, we only show the trans-Niño index (TNI), which captures the central Pacific variability (Trenberth and Stepaniak 2001). This particular ENSO flavor has been shown to be of more relevance to Southern Hemisphere variability (e.g., Trenberth and Stepaniak 2001; Lim et al. 2021b), and in particular the SH stratosphere (Hurwitz et al. 2011; Lin et al. 2012; Hurwitz et al. 2014; Yang et al. 2015), but our results are similar to other ENSO indices. To measure the strength and phase of the IOD, we use the dipole mode index (DMI; Saji et al. 1999). Just like before, we produce PDFs of the index values across events for the early, mature, and late stages (Fig. 5). In addition, we

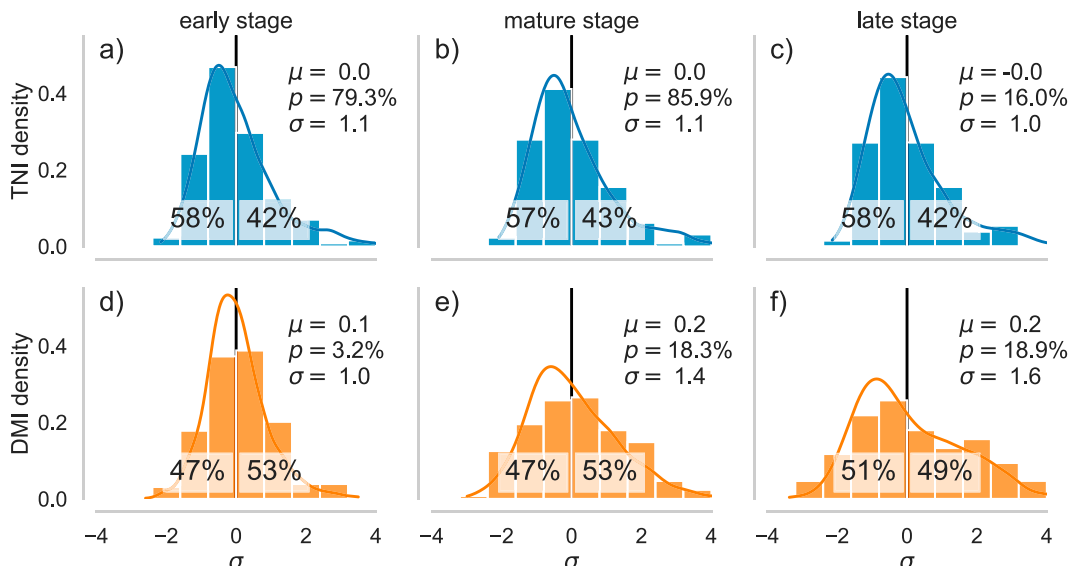


FIG. 5. PDFs of (a)–(c) ENSO via the trans-Niño index (TNI) and (d)–(f) the IOD via the dipole mode index (DMI) for (left) early, (center) mature, and (right) late stages. The bars represent histograms of all SSWs, while the continuous lines represent kernel density estimates (KDEs) from 1610 randomly chosen non-SSW years with the same seasonal distribution as the SSWs. As in Figs. 3 and 4, the percentages show the fraction of SSWs with negative or positive sign. The mean value of each PDF is denoted as μ , and the p value corresponds to a two-sided Kolmogorov–Smirnov test comparing the SSW (bars) to the climatological distributions (lines).

compare the SSW-related PDFs (bars) to the climatological distributions (section 2; continuous lines) and test the similarity of the two distributions (SSW-related vs non-SSW) with a Kolmogorov–Smirnov test (p values given in Fig. 5).

For ENSO, we do not see any particular signal in either stage of the SSW life cycle (Fig. 5, top). In particular, the mean value remains neutral in all stages and the distribution itself is statistically similar to the climatological distribution (p value $\geq 16\%$ for all stages). Hurwitz et al. (2014) report that most CMIP5 models underrepresent stratospheric ENSO teleconnections, and it may be possible that our model similarly underestimates the role of ENSO in the SSW life cycle. However, we show in appendix B that the TNI teleconnections are well represented in the troposphere and the TNI teleconnection to the SH polar vortex is not inconsistent with ERA5. While Hurwitz et al. (2011), Lin et al. (2012), Hurwitz et al. (2014), and Yang et al. (2015) report a warming of the lower polar stratosphere in relation to a positive TNI, we find that those results are not robust when considering more recent reanalysis data (appendix B). In particular, when regressing the strength of the SH polar vortex onto the TNI in any reanalysis over the period 1979–2021, we find that a positive TNI results in a slightly stronger polar vortex (Fig. B3 and similar regressions with reanalysis products available within the NOAA Web-based Reanalyses Intercomparison Tools (WRIT) at <https://psl.noaa.gov/data/writ/>). Thus, we conclude that while tropical Pacific SSTs may have an impact on the mean state of the Antarctic polar vortex as reported elsewhere, they do not play a significant role in the life cycle of SSWs in the SH.

In contrast to ENSO, the DMI shows a slightly positive mean during the early stage, and the distribution is significantly different from climatology (Fig. 5d). While the mean shifts toward slightly more positive values after the early stage, the distribution is not significantly different from climatology anymore (Figs. 5e,f). In addition, while the mean DMI value is positive at the late stage, slightly more events have negative values (51% vs 49%) by that stage, and the peak of the distribution is below zero as well (Fig. 5f). Both of these features are also present in the climatological distribution (cf. bars to lines). Thus, we conclude that there is a tendency toward a positive Indian Ocean dipole prior to onset (early stage), which could be seen as a precursor to SSWs, although we also note that almost half of the events (47%) do not have a positive DMI during the early stage.

4. Stratosphere–troposphere coupling

We first discuss the evolution of the SAM index, which we define as the standardized area-weighted polar cap (south of 60°S) geopotential height anomaly at each pressure level (Baldwin and Thompson 2009). As a warmer and weaker polar vortex translates into a positive geopotential height anomaly but a negative SAM, we switch the sign to follow traditional conventions (i.e., a positive geopotential height anomaly corresponds to a negative SAM index).

The evolution of the SAM in lag–pressure space follows the classic pattern of a slow downward propagation of an initial upper stratospheric signal (Thompson et al. 2005; Shen et al. 2022; Lim et al. 2021a), although it is much slower than for SSWs in the Northern Hemisphere (Fig. 6a). While the zonal

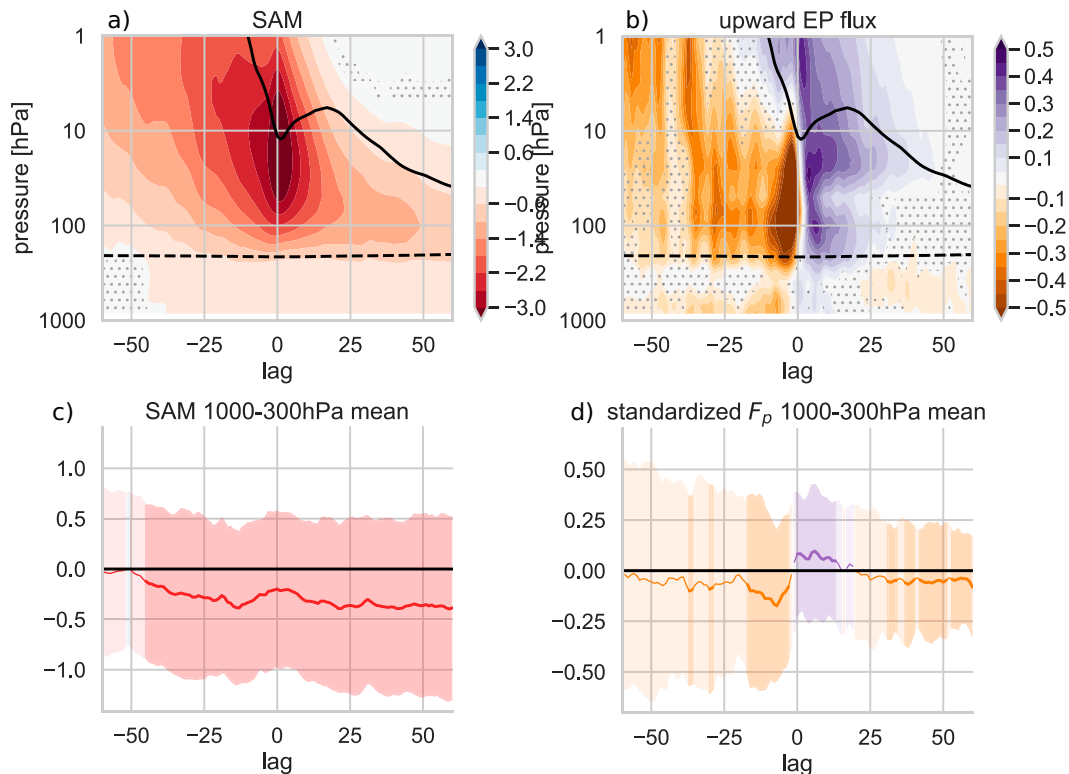


FIG. 6. Lag–pressure composites of (a),(c) Southern Annular Mode index and (b),(d) standardized vertical wave-1 EP flux (negative means upward). The solid black line in (a) and (b) shows the zero contour of zonal mean zonal wind averaged between 70° and 50°S , and the dashed line shows the tropopause averaged between 90° and 20°S . EP flux is computed following Jucker (2021b) and standardized at each pressure level following Jucker (2016), cosine-latitude weighted and averaged from 20° to 90°S . Statistically insignificant regions (95% level) are hatched. The bottom panels show vertically averaged values between 1000 and 300 hPa for the mean (bold) and cross-event standard deviation (shading). Not significant anomalies are drawn with lighter shading and a thin line.

mean zonal wind decelerates quickly within two weeks of the onset date (continuous line), the SAM index anomaly is statistically significant throughout the stratosphere already 60 days before onset, and takes about one month to descend from 10 to 100 hPa. The slower descent of the stratospheric signal in the SH compared to SSWs in the NH has been reported earlier (Shen et al. 2022) and is consistent with the generally slower time scales of the evolution of the SAM compared to its NH counterpart (Gerber et al. 2008; Kim and Reichler 2016). The tropospheric anomaly is statistically significant from about 40 days before onset and remains significantly negative beyond 60 days after onset (i.e., for a total of more than three months) (Fig. 6c). An interesting feature is the period of less negative tropospheric SAM around onset (between lags -10 and $+10$; Fig. 6c), which might be related to the “fast response” of the troposphere to increased stratospheric temperatures described by Jucker and Goyal (2022).

To diagnose wave driving of the SSW, we analyze the wave-1 component of standardized vertical Eliassen–Palm (EP) fluxes averaged over the SH extratropics [computed following Jucker (2021b) and standardized following Jucker

(2016)], as total stratospheric EP flux is dominated by wave 1 (Fig. 8, discussed below). Even so, wave-1 EP flux shows few statistically significant values in the troposphere, except over periods of about two weeks before (upward) and after (downward anomalies) onset (Figs. 6b,d). However, there is a persistent upward anomaly close to the surface that is significant from lag -50 , and that corresponds to the wave-1 surface perturbations discussed in Figs. 1 and 2. While these mean anomalies might suggest that there is constant EP flux forcing for long periods of time, Fig. 7 suggests that this is not the case: It shows that the negative (upward) mean during the early stage is a result of averaging over multiple events of strong one- to two-week “bursts” of upward EP flux (Figs. 7a,b) that are not counteracted by similar periods of downward anomalies (Figs. 7d,e). Such preonset bursts are consistent with previous work suggesting that SSW forcing does not necessarily need a single strong “burst” of upward EP flux, but rather the time-integrated amount of wave forcing is important (Polvani and Waugh 2004; Sjoberg and Birner 2012; Jucker 2016; Birner and Albers 2017; Reichler and Jucker 2022).

In contrast to the troposphere, the stratosphere shows statistically significant values of anomalously upward EP flux

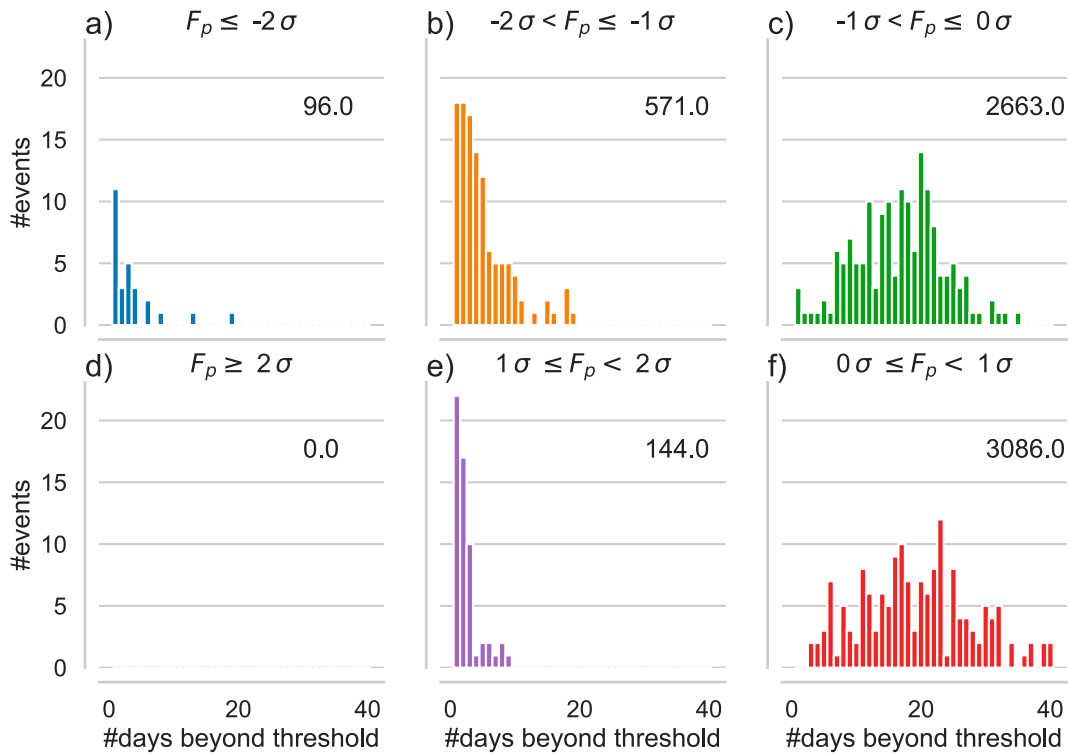


FIG. 7. Histograms of number of days spent within given threshold ranges (titles) of hemispheric-mean upward EP flux in pressure coordinates (F_p) during the early SSW stage (from lags -60 to -20 ; i.e., 40 days) at 700 hPa. (a)–(c) Upward anomalies (i.e., negative F_p) and (d)–(f) downward anomalies (i.e., positive F_p). The numbers in each panel give the total event days, i.e., the integral below each histogram. The total number of events is 161. The histograms suggest that the significant upward mean near the surface in Fig. 6b is due to individual periods of strong upward F_p (beyond 1σ), which typically last for 1–2 weeks [as in (a) and (b)]. In contrast, moderate to weak events (below 1σ) are more evenly distributed between either sign [as in (c) and (f)].

almost everywhere at negative lags, and while the significant anomalies start almost exactly at the tropopause, their upper limit shows a downward tendency. This is in agreement with the zonal mean zonal wind decelerating and the steady downward propagation of the SAM described above.

Furthermore, the constant wave forcing in the stratosphere causes the polar vortex to slowly but steadily weaken, and by about two weeks prior to onset, the polar vortex reaches a state where strong tropospheric EP flux can penetrate the stratosphere and ultimately cause the SSW (Limpasuvan

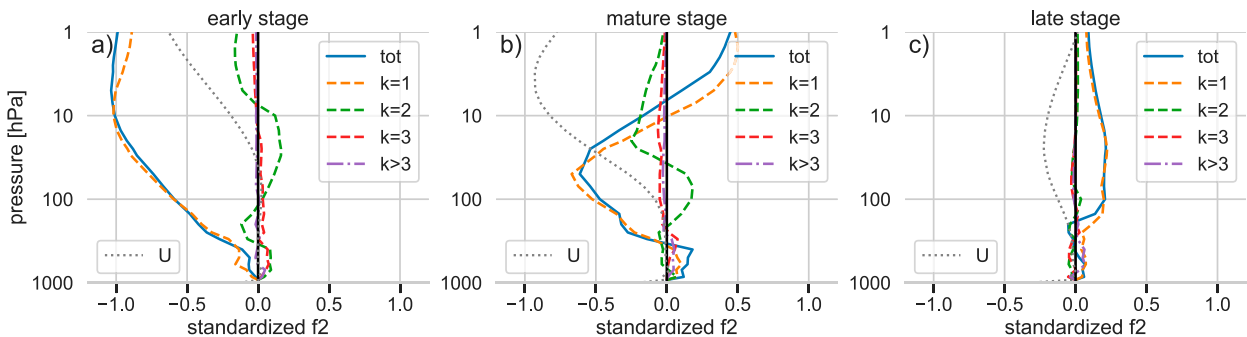


FIG. 8. Zonal mean zonal wind anomalies (gray dotted) and vertical EP flux anomalies by wavenumber, divided into all waves (blue, continuous), planetary wavenumbers 1–3 (colors, dashed), and synoptic-scale waves (purple, dash-dotted). All quantities are area-weighted and averaged from 85° to 60° S, and divided into the (a) early, (b) mature, and (c) late stages. Zonal mean zonal wind is plotted from -30 to $+30 \text{ m s}^{-1}$ (axis labels not shown), and the x labels correspond to standardized EP fluxes. Note that like in Fig. 7, we plot F_p in pressure coordinates, i.e., negative means upward (Jucker 2011b).

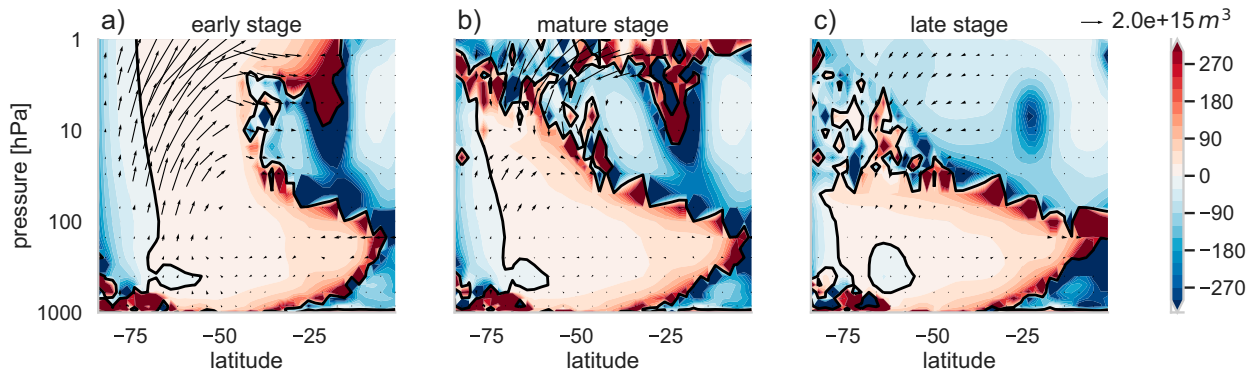


FIG. 9. Refractive index n^2 (shading) and flux vector anomalies (arrows) for the (a) early, (b) mature, and (c) late stages and for wave-number-1 waves. The black line denotes $n^2 = 0$, arrows are computed and scaled following Jucker (2021b), and scale is indicated by the arrow on the right.

et al. 2004; Albers and Birner 2014; Jucker and Reichler 2018).

Stratospheric EP flux anomalies are almost entirely due to wavenumber 1 (Fig. 8). As the negative polar vortex anomalies start from the upper stratosphere and propagate downward (gray dotted line in Fig. 8), wave anomalies likewise peak at lower and lower heights, but always in the stratosphere [note that negative upward EP flux values mean anomalously upward as we use pressure coordinates following Jucker (2021b)]. The downward motion of the peak anomalous EP flux strength at negative lags follows the negative zonal mean zonal wind anomalies, as the refractive index becomes negative due to the strong deceleration of the polar vortex (Fig. 9). This is consistent with the interpretation that progressive wave–mean flow interactions happen at the lower edge of the polar vortex where the refractive index becomes negative, and thus weaken the polar vortex below the previous center of deceleration, causing a downward migration of the wind anomalies (Plumb and Semeniuk 2003).

The evolution of the refractive index n^2 for wavenumber 1 shows how the breakdown of the polar vortex causes the channel of upward wave propagation to collapse from its equatorward flank and from the top (left to right in Fig. 9), resulting in stratospheric EP fluxes being confined to lower and lower heights, confirming the above picture using zonal mean zonal wind. We note here that given that all SSWs occur in September or later, the late stage here includes the seasonal breakdown of the polar vortex.

Another interesting part of the SSW life cycle at the interface between the stratosphere and the troposphere is a change of the tropopause height, with a lower tropopause at high latitudes and a higher tropopause at low latitudes (Fig. 10). This is consistent with adiabatic heating and cooling associated with a stronger stratospheric meridional overturning circulation with anomalous upwelling in the tropics and downwelling at high latitudes. In the tropics, the tropopause rises by up to about 300 m, whereas it decreases between 500 m and 2 km at high latitudes.

5. Stratospheric evolution

a. 2D momentum analysis

The only observed major SSW in the SH was a vortex split event (Roscoe et al. 2005; Newman and Nash 2005; Stolarski et al. 2005), while the only other similarly strong event in 2019—although technically not a major SSW—was a displacement event (Safieddine et al. 2020; Shen et al. 2020; Lim et al. 2021a). We now analyze the polar vortex geometry of all SSWs in our simulation via two-dimensional moment analysis. Following Seviour et al. (2013), we compute the polar vortex centroid latitude and aspect ratio using 10-hPa geopotential height. In their work, these authors define an SSW to be a displacement event if the centroid latitude remains poleward of 66° latitude (north in their case) for at least seven days, and a split event if the aspect ratio remains greater than 2.4 for at least seven days. While we do not use the 2D moments to

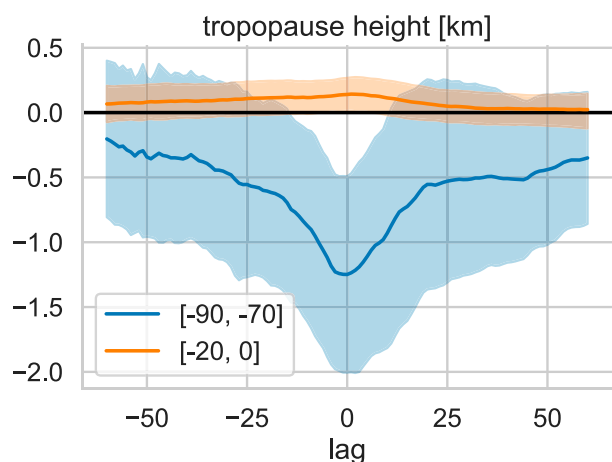


FIG. 10. Tropopause height anomalies as a function of lag for low latitudes (20°S to the equator; orange) and high latitudes ($90^\circ\text{--}70^\circ\text{S}$; blue). Solid lines show the mean and shading the standard deviation across events. Tropopause calculated following Reichler et al. (2003).

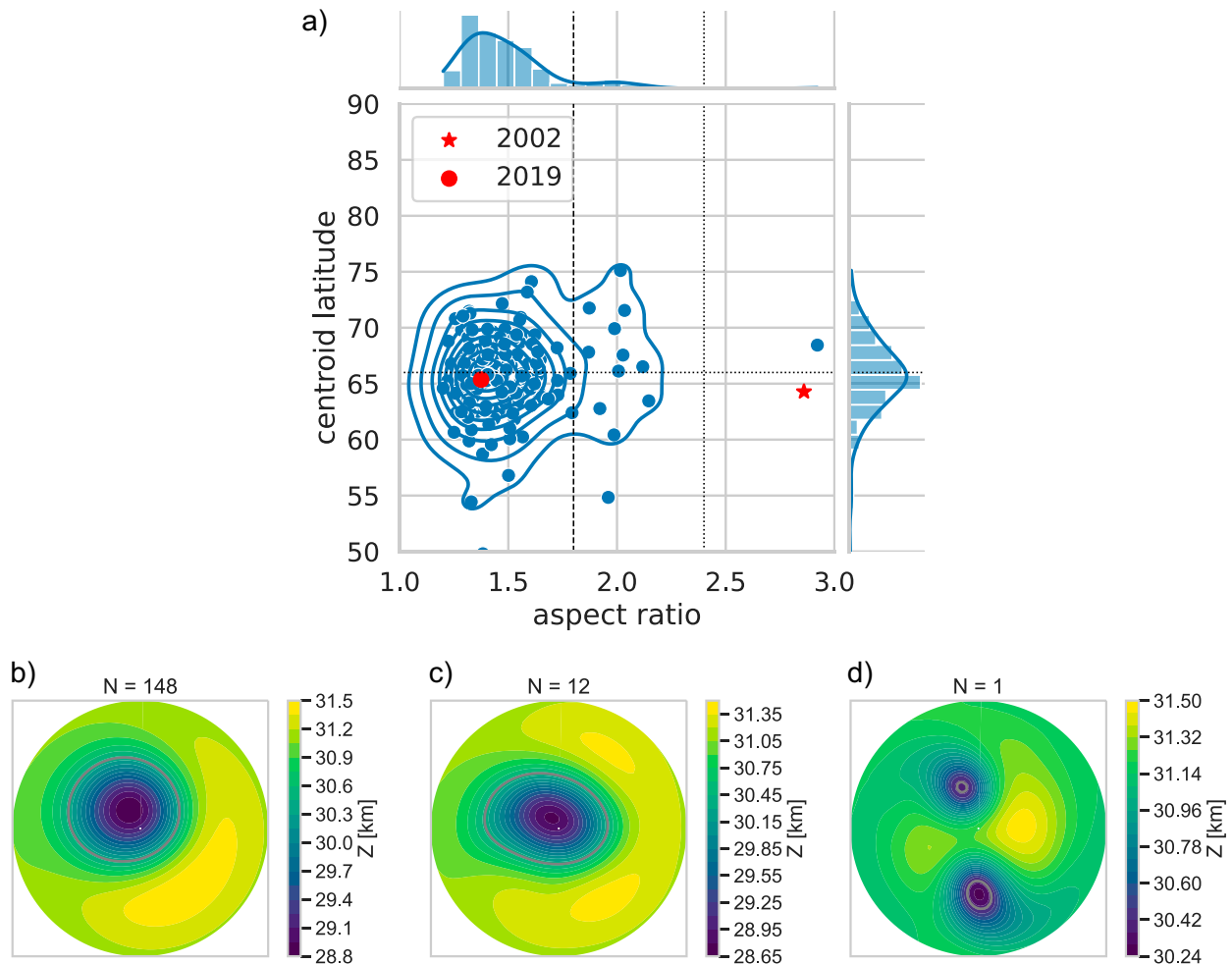


FIG. 11. 2D vortex moment analysis for all SSWs. (a) Distribution in aspect ratio–centroid latitude space, showing an almost Gaussian distribution around an aspect ratio of about 1.4 and a centroid latitude of 66°S, which is similar to the observed 2019 minor SSW (red circle). Blue dots show a scatterplot of individual events and lags, while the blue contours define a kernel density estimate of the same data. Thin gray dotted lines show the thresholds of 2.4° and 66°S from [Seviour et al. \(2013\)](#) for the definition of split and displacement events in the Northern Hemisphere. In our analysis of the SH, there seems to be a secondary population of aspect ratios between 1.8 (black dashed line) and 2.4 (gray dotted vertical line). (b) The composite of the population with aspect ratios below 1.8 and corresponds to displacement events. (c) Events with aspect ratios between 1.8 and 2.4; these do not correspond to a split vortex per se, but include two distinct geopotential height maxima around 30° and 150°E. (d) There is only one single event in the simulation similar to the vortex split of 2002 (with an aspect ratio above 2.4). The composites in (b)–(d) are created by averaging over all events and lags where the respective conditions on aspect ratio are satisfied. The solid gray lines show the 30.4-km lines used to detect the vortex edge in the momentum calculations, and the title shows the number of events in the composite.

detect SSWs, we compute the centroid latitude and aspect ratio for all SSWs and at all lags (we define the vortex edge as the 30.4-km contour at 10 hPa) and compute the maximum value of the 7-day rolling minimum aspect ratio (henceforth simply “aspect ratio”) as well as the minimum value of the 7-day rolling maximum centroid latitude (henceforth simply “centroid latitude”). This allows an assessment of potentially more appropriate threshold values for detecting SH events.

The distribution in centroid latitude–aspect ratio space shows that all but one SSW in our simulation would be defined as a displacement event (Fig. 11a). We also note that the

threshold of 66°S would probably be too constraining, and a threshold of 55°–60°S would be more appropriate. Compared to the simulated SSWs (blue dots and contours), the 2019 event is right in the center of the distribution, while only one simulated SSW has an aspect ratio similar to the 2002 event.

Interestingly, there seems to be a secondary maximum in the aspect ratio distribution around a value of 2.0. A composite of all SSWs within that secondary peak (aspect ratio between 1.8 and 2.4; Fig. 11c) reveals that rather than a split of the polar vortex itself (blue area), these events correspond to a structure of two peaks of anomalously high geopotential height outside of the polar vortex (yellow colors). In contrast,

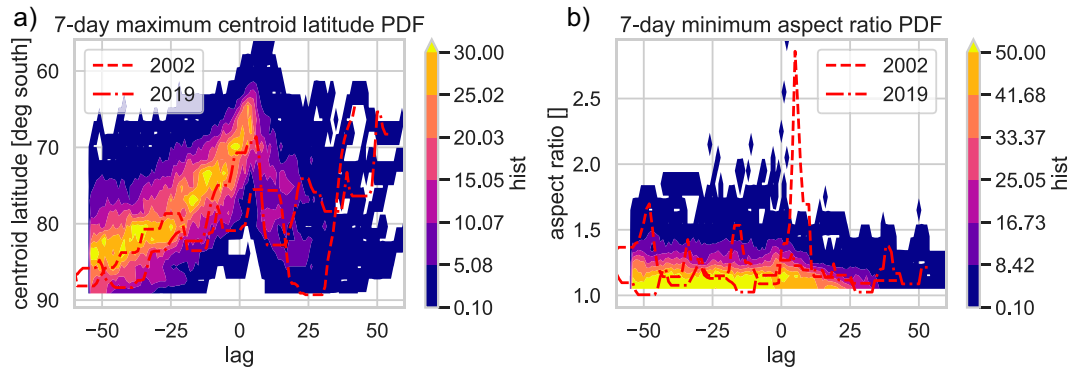


FIG. 12. Evolution of the PDF of (a) centroid latitude and (b) aspect ratio as a function of lag. As in Fig. 11 the 2019 event follows the model distribution very closely.

the composites of SSWs with aspect ratios lower than 1.8 (Fig. 11b) and the one event with an aspect ratio higher than 2.4 (Fig. 11d) show the traditional geometries of displacement and split events. From our analysis it is not possible to discern whether the population of midrange values in aspect ratios are due to a reluctance of our model to create splitting events, or whether it is a consequence of the intrinsic differences between the two hemispheres.

Another way of analyzing the polar vortex geometry around the onset date of SSWs is to construct the distributions of both centroid latitude and aspect ratio across events at each lag (Fig. 12). Again we see that the observed 2019 event follows the evolution of the centroid latitude of our simulated events (red dashed line following the distribution peak in Fig. 12a), with a slow decrease prior to onset and a fast reset at positive lags. The 2019 event also follows the aspect ratio of most SSWs in our simulation, and the strong but short peak of the 2002 split SSW is replicated by one event in the simulation, as discussed above (Fig. 12b, dashed red line versus blue dots around lag 0). To summarize, most simulated SSWs are similar to the 2019 observed event in terms of 2D moment polar vortex analysis, looking like a displacement event, and only

one of the 161 events has an aspect ratio similar to that of the 2002 observed event. There seems to be a small population of SSWs at aspect ratios close to 2.0, which show a distinct geometry featuring two highs outside of the polar vortex, but it is not clear whether such events should be expected to occur in the real atmosphere or whether they are the consequence of a model bias.

b. Final warming date and tropical winds

SSWs also have an effect on the date of the final polar vortex breakdown (or final warming; Fig. 13a; all years in blue/shaded, SSW years in orange/solid), even if we find no change in mean breakdown date as reported in a few observational studies (Lim et al. 2018). It is possible that the increase in stratospheric ozone during SSWs—which is not included in our model—warms the polar vortex beyond the dynamical effects, causing an earlier breakdown (Jucker and Goyal 2022), or that there is a difference between major SSWs studied here and the weaker events found in observations. Nevertheless, while the mean date remains at day of year 324 during years with major SSWs (20 November, denoted by μ in Fig. 13a), we still see a difference in the final warming distribution as

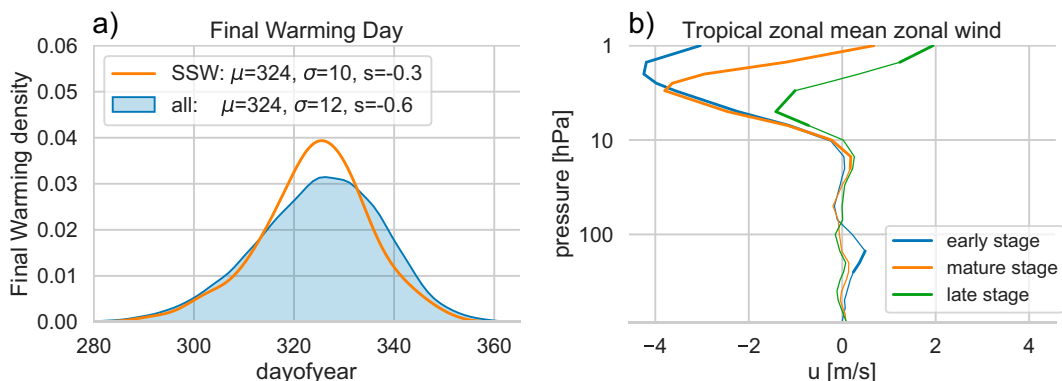


FIG. 13. (a) PDF of final warming date for (blue) all years and (orange) years with SSWs only. The legend includes information on mean day of year (μ), standard deviation (σ), and skewness (s). (b) Composites of tropical mean (5°S – 5°N) zonal mean zonal wind for the early (blue), mature (orange), and late (green) stages. Thick lines mean that anomalies are statistically significant at the 95% level.

TABLE A1. Definitions of regions in Figs. 3 and 4.

Acronym	Long name	Zonal extent	Meridional extent
SAF	Southern Africa	14°–35°E	34.5°–17°S
WAUS	Western Australia	113°–135°E	35°–14°S
EAUS	Eastern Australia	135°–155°E	39°–17°S
NZ	New Zealand	166.5°–178.5°E	47°–34.5°S
SSA	Southern South America	73°–62°W	55°–34°S
IA	Indian sector Antarctica	30°–110°E	90°–65°S
PA	Pacific sector Antarctica	160°E–80°W	90°–65°S

both the standard deviation (σ) and the skewness (s) decrease. A Kolmogorov–Smirnov test on the two distributions gives a p value of 7%, meaning that the final warming date distributions between years with and without SSWs are significantly different at the 93% level, and the main difference is that there are fewer late final warmings in years with SSWs.

Finally, the zonal-mean zonal wind composites show persistent easterly winds in the deep tropics above 10 hPa (5°S–5°N; Fig. 13b). While our model does not produce a quasi-biennial oscillation (QBO), in the Northern Hemisphere there is a known link between SSWs and the zonal wind structure in the tropics (Holton and Tan 1980). Given that our model produces an SSW frequency that is consistent with observations and other models (Jucker et al. 2021; Wang et al. 2020), and that the upper stratospheric zonal wind anomalies are statistically significant during the early and mature stages, we assume that the upper stratospheric easterlies are part of the life cycle of SSWs in the SH. However, more work is required to investigate this relationship.

6. Summary and conclusions

Stratospheric sudden warmings (SSWs) are rare in the Southern Hemisphere (SH) (Jucker et al. 2021), but are thought to be capable of inducing anomalous weather at the surface on the seasonal time scale (Thompson et al. 2005; Lim et al. 2018). Due to their rareness, it is difficult to obtain a physical understanding of their life cycle, including possible precursors, dynamical evolution, and surface impact. We used data from a nearly 10 000-yr simulation with a stratosphere-resolving version of the coupled climate model CM2.1 (Staten and Reichler 2014), which has been shown to faithfully reproduce tropical (Wittenberg et al. 2006), extratropical (Reichler and Kim 2008), and stratospheric climate and its variability (Horan and Reichler 2017) (see also appendix B for further model evaluation). Thanks to the long simulation, we can focus on major SSWs, defined following one of the simplest and most widely used definitions (Charlton et al. 2007).

Our composite life cycle analysis shows the following:

- The Indian Ocean dipole has a slight tendency toward positive values before the onset of SSWs, whereas ENSO does not seem to be important (Fig. 5).
- Extratropical sea level pressure, surface temperature, and precipitation anomalies strongly project onto the negative

phase of the Southern Annular Mode already *before* the onset date (Fig. 6). However, there is a strong wave-1 component in sea level pressure anomalies before onset, with a strong weakening of the Amundsen Sea low. These anomalies become much more zonally symmetric after onset (Fig. 1).

- Regions with the strongest pre-existing precipitation anomalies are generally located around the Pacific basin, with drier than usual conditions over Eastern Australia, and wetter than usual conditions over New Zealand, Antarctica, and southern South America. While Australia experiences a shift toward even drier conditions after onset, New Zealand does not see a significant shift, the Antarctic coast in the Pacific sector also sees a drying, but southern South America experiences slightly more precipitation (Fig. 3).
- Pre-SSW surface temperature anomalies are statistically significant over Eastern Australia (warmer than usual) and southern South America (colder than usual). The largest shifts between pre- and post-SSW occur over New Zealand (colder), southern South America (colder), and over Antarctica, while the Australian continent remains warmer than usual, and the temperature anomalies over the Pacific sector of Antarctica become neutral post-SSW after being positive pre-SSW.
- In the atmosphere, the life cycle follows the evolution familiar from the Northern Hemisphere, although progression is slower: The upper stratospheric SAM index is negative more than 60 days prior to onset, and those anomalies travel downward over several months. However, tropospheric SAM becomes negative about one month before onset, in line with above discussed surface anomalies (Fig. 6a). Upward EP flux anomalies are dominated by wave 1 and follow zonal mean zonal wind anomalies downward from the upper to the lower stratosphere (Fig. 8). Besides the stratosphere, they are also statistically significant near the surface, and throughout the troposphere during the last two weeks before onset (Fig. 6b).
- The events are almost exclusively displacement events, with only one splitting event but a small population of “inverse splits,” that is, events where the region of high geopotential height around the low-height center forms two distinctive maxima (Fig. 11).
- While the mean final warming date does not change between years with and without SSWs (possibly due to the missing warming effect of interactive ozone in the model), the PDF of final warming dates in years with SSWs is much narrower and less skewed than in years without SSW (Fig. 13a), meaning there are fewer late final warmings in years with SSW.
- Pre-SSW, the tropical winds show strong easterly anomalies above 10 hPa, which decay during SSW evolution (Fig. 13).
- The high-latitude tropopause is 0.5 to 2 km lower at onset than its climatological height, which might have dynamical implications for stratosphere–troposphere coupling, which will be examined in future work (Fig. 10).

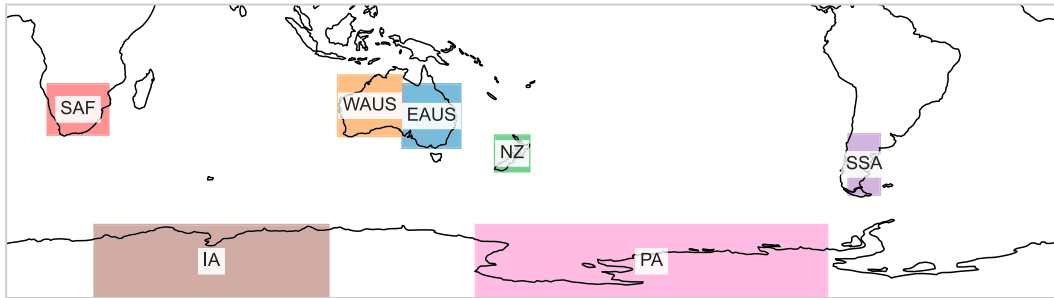


FIG. A1. Rectangular regions used for producing the PDFs of Figs. 3 and 4.

To conclude, our study shows that many of the typical surface anomalies associated with SSWs are already present long before the onset date, and that in particular the tropical Indian Ocean and the region around the Amundsen Sea low stand out as precursors for SSWs in the SH. There is, however, still much to study in terms of the dynamics of SSWs in the SH.

Acknowledgments. M.J. was supported by the Australian Research Council (ARC) Grant FL150100035 and the ARC

Centre of Excellence for Climate Extremes, which is supported by the Australian Research Council via grant CE170100023. T. R. acknowledges support from NSF Grant 1446292. We also acknowledge the Center for High Performance Computing at the University of Utah and the National Computational Infrastructure in Canberra for providing compute infrastructure and computing time. This research used resources of the National Energy Research Scientific Computing Center, a DOE Office of Science User Facility supported by the Office of Science of the U.S. Department

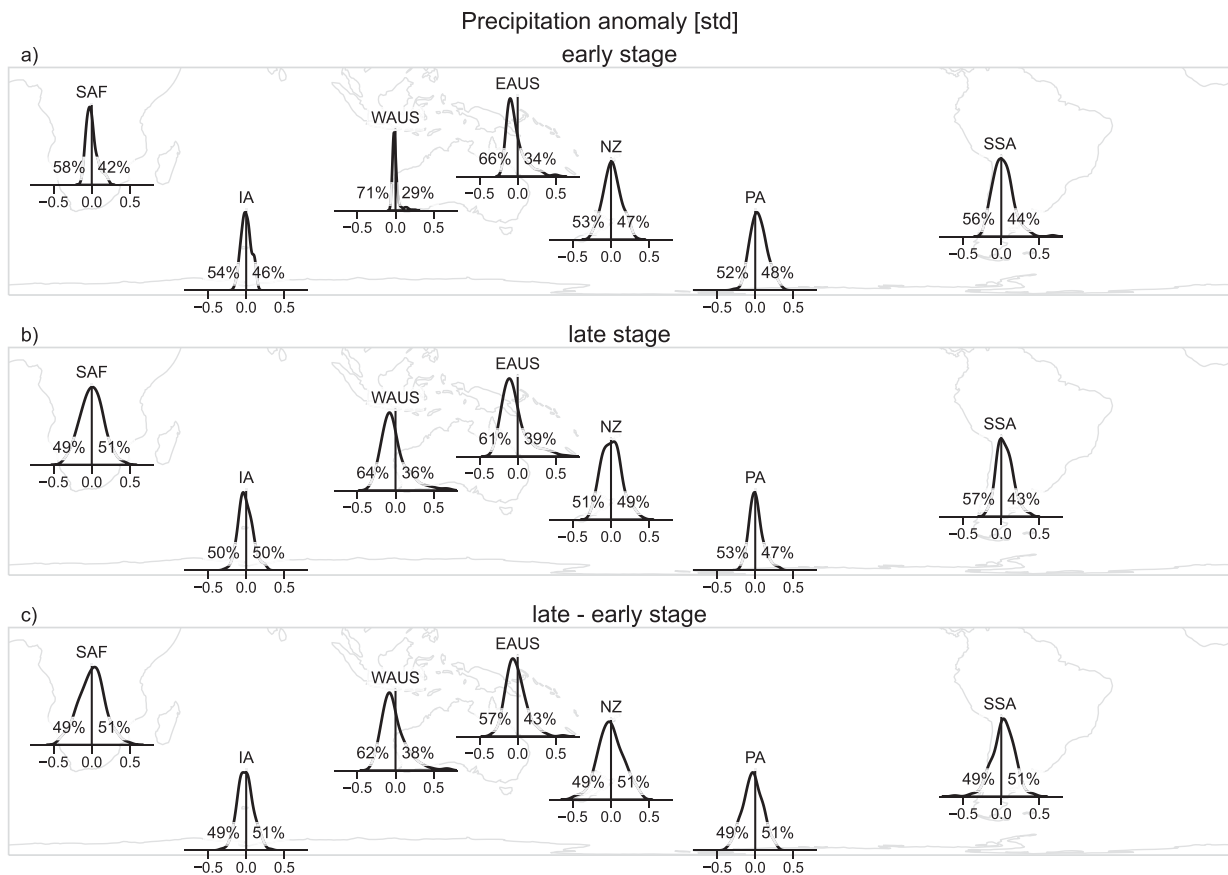


FIG. A2. As in Fig. 3, but for years without SSWs. Given the PDFs show anomalies, their mean values are all zero and are therefore removed from the inset titles.

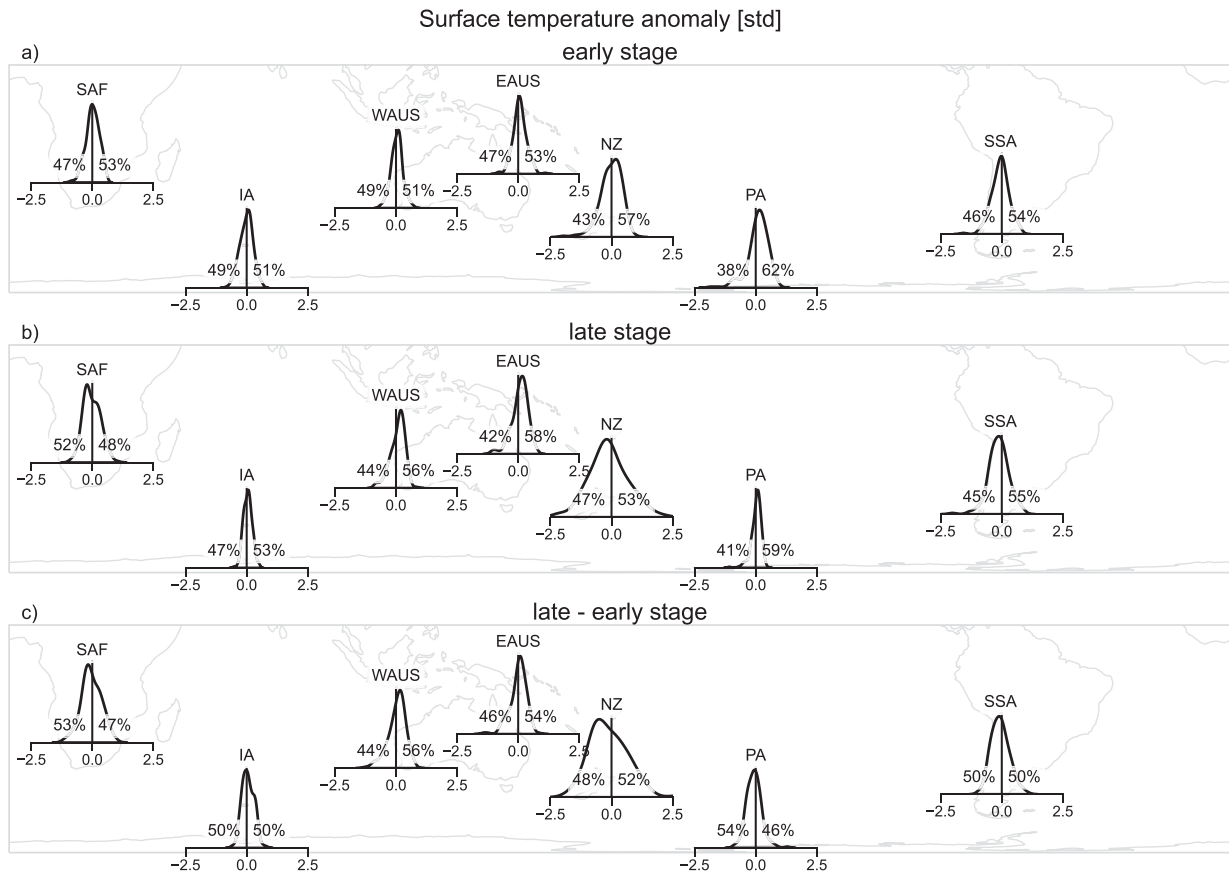


FIG. A3. As in Fig. 4, but for years without SSWs. Given the PDFs show anomalies, their mean values are all zero and are therefore removed from the inset titles.

of Energy under contract DE-AC02-05CH11231 using NERSC Award BER-ERCAP0020431. We thank two anonymous reviewers and Isla Simpson for their helpful and constructive comments. This work used the xarray (Hoyer and Hamman 2017) and aostools (Jucker 2021a) packages. The authors declare no conflicts of interest.

Data availability statement. All data and python scripts necessary for the reproduction of the figures in this paper are available at <https://doi.org/10.5281/zenodo.6609584>.

APPENDIX A

Regional Impacts

a. Region definitions

The regions used in Figs. 3 and 4 are defined as rectangular boxes in longitude–latitude space as per Table A1. For illustration, Fig. A1 shows the relevant boxes on a map.

b. PDFs for non-SSW years

The PDFs in Figs. 3 and 4 are non-Gaussian, and we show in Figs. A2 and A3 the PDFs of the same variables

within the same regions for years without SSW. These PDFs are constructed by randomly choosing 1610 years without SSWs (chosen to be 10 times more than the number of SSWs). To account for the seasonal variation included in the SSW distribution, we chose the same dates as the SSW years (e.g., for every specific SSW onset date, there are 10 instances with the same day of the year), but during years without SSWs. These PDFs are then compared to the SSW PDFs with a Kolmogorov–Smirnov test for statistical significance. This explains why some of the PDFs in Figs. 3 and 4 are statistically insignificant from climatology, even if they are non-Gaussian.

APPENDIX B

Model Evaluation

Besides the extensive model evaluation for ENSO and ocean circulation (Wittenberg et al. 2006; Gnanadesikan et al. 2006) as well as atmospheric behavior (Horan and Reichler 2017; Jucker and Reichler 2018; Jucker et al. 2021), we present here further evaluation against ERA5 reanalysis aimed at confirming the reproduction of the most important features involved in stratosphere–troposphere coupling in the SH.

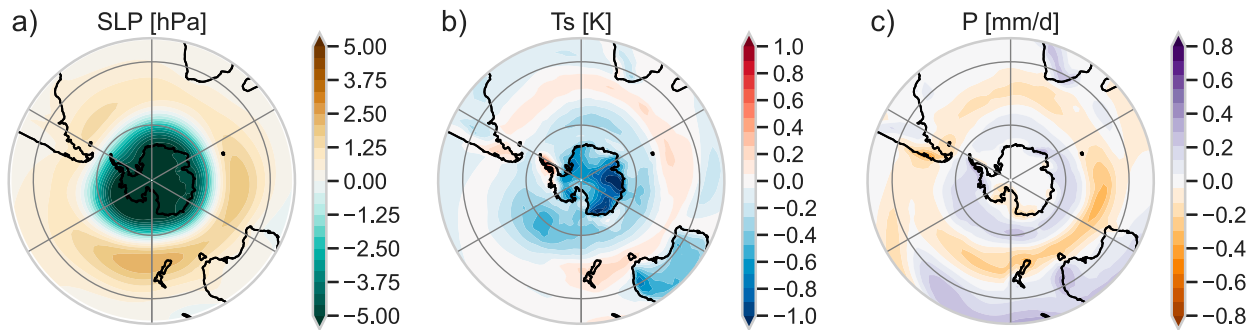


FIG. B1. (a) First empirical orthogonal function of sea level pressure, whose principal component (PC1) serves as the Southern Annular Mode index for this figure. (b) Regression of PC1 onto surface temperature, and (c) precipitation. These panels are produced with monthly model data and can be compared to Southern Annular Mode impact studies, such as Gillett et al. (2006), revealing a faithful reproduction of the SAM and its teleconnections in our model.

a. Southern Annular Mode

Sections 3 and 4 compare the surface impact and the stratosphere–troposphere evolution to the known impacts of the negative phase of the Southern Annular Mode. To confirm that the model faithfully reproduces impacts of the SAM on sea level pressure, surface temperature, and precipitation, Fig. B1 shows the regressions of surface temperature and precipitation onto the first principal component of sea level pressure (Figs. B1b,c). Figure B1a shows the first empirical orthogonal function of mean sea level pressure, which is here taken as defining the SAM.

b. ENSO

In section 3c we find that ENSO does not play an important role in the forcing of SSWs, which might be surprising given that previous literature established a link between tropical Pacific SSTs and the polar vortex in the SH (Hurwitz et al. 2011; Lin et al. 2012; Hurwitz et al. 2014). Therefore, we here evaluate our model’s capacity to reproduce ENSO teleconnections.

1) TROPOSPHERIC TELECONNECTIONS

The model faithfully reproduces the extratropical teleconnections of central Pacific ENSO, which we diagnose as the

regression of 300-hPa geopotential height onto the trans-Niño index (TNI) in September–November, compared to ERA5 (Fig. B2). We focus on the upper troposphere as this is the most important region for stratosphere–troposphere coupling and SSWs. The regressions show very similar amplitude, and only small biases in the location of the highs and lows in the model.

2) STRATOSPHERIC TELECONNECTIONS

Previous work reports a warming of the Antarctic stratosphere during central Pacific El Niño events (Hurwitz et al. 2011, 2014; Yang et al. 2015), although these studies are based on relatively few events and most results are only statistically significant in the lower stratosphere. Nevertheless, we compare the regression of monthly mean zonal mean zonal wind anomalies onto the TNI September–November in Fig. B3. For our analysis, we created a bootstrap ensemble by subsampling each dataset (each row in Fig. B3) 1000 times with replacement, resulting in an ensemble of 1000 members \times 3 months \times 21 years from (top row) the full CM2.1 simulation, (middle row) ERA5 between and including 1979–99, and (bottom row) ERA5 between and including 2000–20. The top two rows (Figs. B3a,c) seem to confirm that there is a tendency toward a slightly weaker zonal mean zonal wind in the lower stratosphere at high

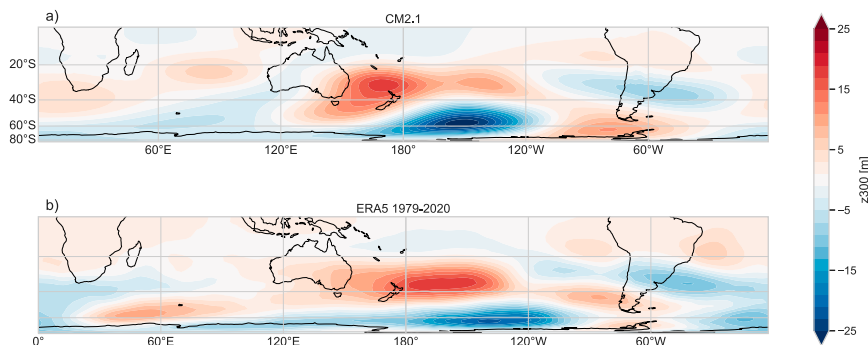


FIG. B2. Regression of TNI onto 300-hPa geopotential height in September–November for (a) CM2.1 and (b) ERA5 (1979–2020).

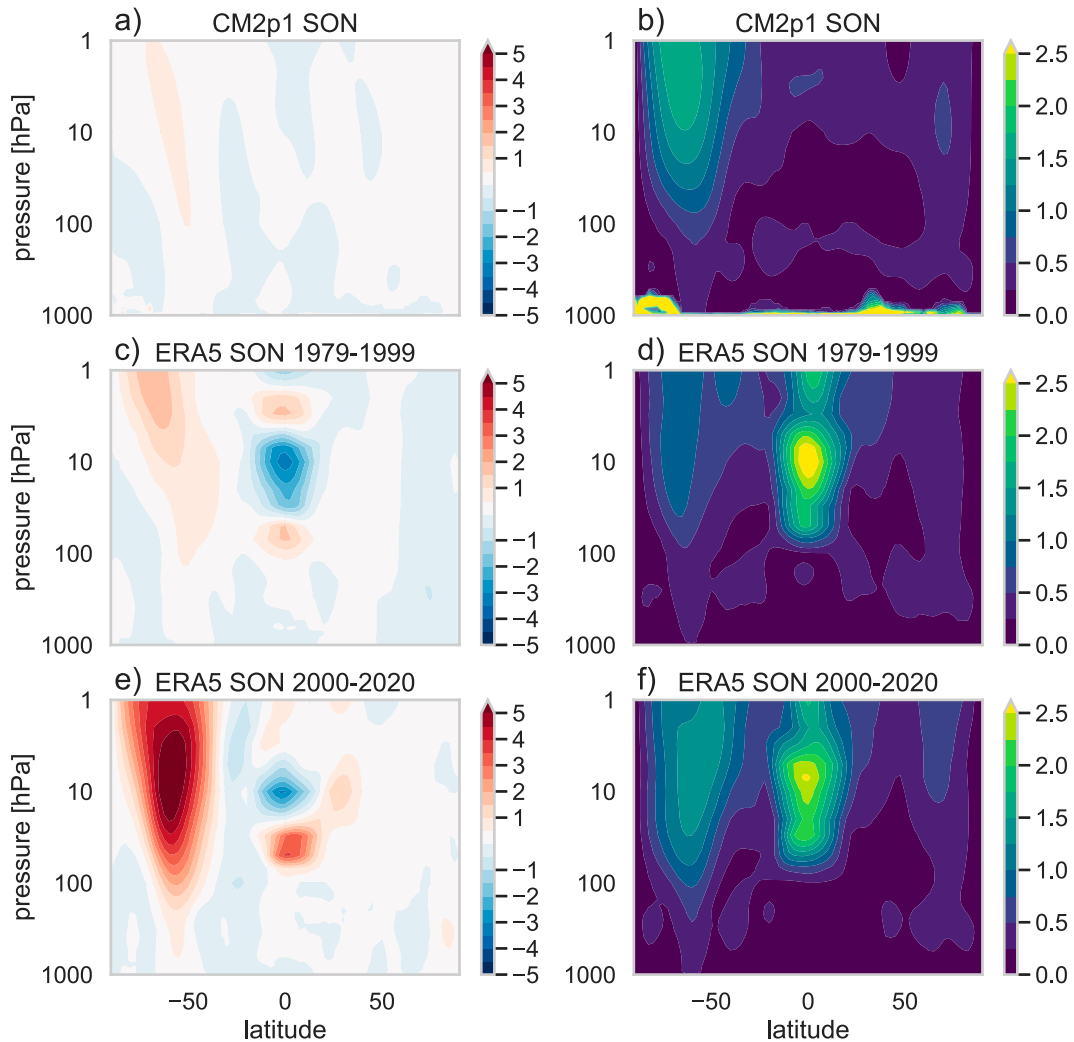


FIG. B3. (left) Regressions of monthly TNI on monthly zonal mean zonal wind anomalies during September–November in (a) CM2.1 and (c),(e) ERA5. We have split the satellite reanalysis period into two equally long subperiods (of 21 years) to illustrate the strong variability in the signal. Model regressions are similar to the earlier period in ERA5, but weaker than the later ERA5 period. In the tropics, ERA5 shows a QBO-like structure which is missing in the model. (right) Standard deviation of the same regressions using bootstrap resampling for (b) CM2.1 and (d),(f) ERA5 (see text for details).

latitudes, similar to [Hurwitz et al. \(2014\)](#), who report a warmer lower Antarctic stratosphere during positive TNI events during the period 1979–2001. However, [Fig. B3](#) also suggests that that result might not be robust in light of the more recent period ([Fig. B3e](#)), and given that the standard deviation across bootstrap members is almost as large as the signal itself (cf. left to right columns). More importantly for this work, the model and reanalysis agree that the polar vortex tends to be slightly stronger with positive TNI. In addition, the amplitude of the TNI-related signal in the stratospheric polar vortex is very small compared to the interannual standard deviation of zonal mean zonal wind, which is on the order of 40 m s^{-1} (not shown) in both ERA5 and CM2.1, and the mean zonal mean zonal

wind perturbation during the life cycle of SSWs, which is about 32 m s^{-1} (not shown).

Thus, considering our analysis of both tropospheric and stratospheric teleconnections related to ENSO in both the model and reanalysis, we conclude that there is little reason to believe that the model has a fundamental bias in representing tropical teleconnections with respect to the life cycle of SSWs. This short analysis does, however, suggest that more work should be done in trying to understand the stratospheric teleconnections of tropical SST forcing.

c. Stationary waves

As shown by [Garfinkel et al. \(2021\)](#), the tropospheric stationary wave structure can have an effect on the strength

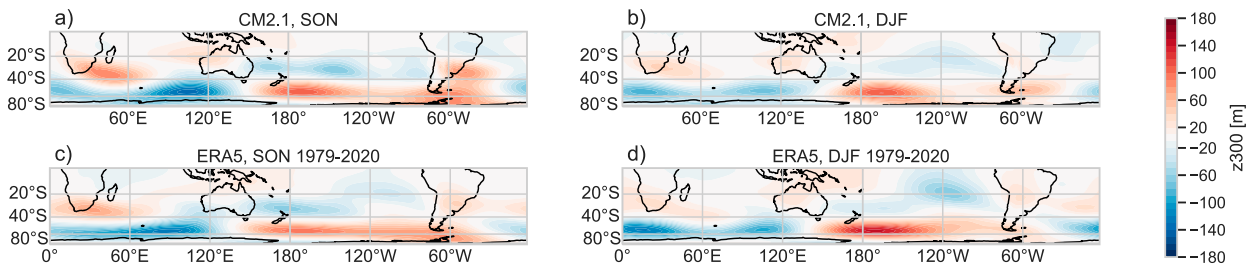


FIG. B4. 300-hPa stationary wave patterns for (a),(b) CM2.1 and (c),(d) ERA5 (1979–2020) during (left) September–November and (right) December–February. The model produces the stationary waves well, with similar amplitudes and only small biases in location of the lows and highs.

of stratosphere–troposphere coupling. Therefore, Fig. B4 compares the stationary waves in the form of September–November climatological zonal asymmetries of 300-hPa geopotential height from CM2.1 to the same quantity from ERA5. Clearly, the stationary waves are well reproduced in both amplitude and structure in all seasons.

REFERENCES

- Albers, J. R., and T. Birner, 2014: Vortex preconditioning due to planetary and gravity waves prior to sudden stratospheric warmings. *J. Atmos. Sci.*, **71**, 4028–4054, <https://doi.org/10.1175/JAS-D-14-0026.1>.
- Baldwin, M. P., and D. W. Thompson, 2009: A critical comparison of stratosphere–troposphere coupling indices. *Quart. J. Roy. Meteor. Soc.*, **135**, 1661–1672, <https://doi.org/10.1002/qj.479>.
- Birner, T., and J. R. Albers, 2017: Sudden stratospheric warmings and anomalous upward wave activity flux. *SOLA*, **13A**, 8–12, <https://doi.org/10.2151/sola.13A-002>.
- Butler, A. H., D. J. Seidel, S. C. Hardiman, N. Butchart, T. Birner, and A. Match, 2015: Defining sudden stratospheric warmings. *Bull. Amer. Meteor. Soc.*, **96**, 1913–1928, <https://doi.org/10.1175/BAMS-D-13-00173.1>.
- Byrne, N. J., and T. G. Shepherd, 2018: Seasonal persistence of circulation anomalies in the Southern Hemisphere stratosphere and its implications for the troposphere. *J. Climate*, **31**, 3467–3483, <https://doi.org/10.1175/JCLI-D-17-0557.1>.
- Charlton, A. J., and Coauthors, 2007: A new look at stratospheric sudden warmings. Part II: Evaluation of numerical model simulations. *J. Climate*, **20**, 470–488, <https://doi.org/10.1175/JCLI3994.1>.
- Charney, J., and P. Drazin, 1961: Propagation of planetary-scale disturbances from the lower into the upper atmosphere. *J. Geophys. Res.*, **66**, 83–109, <https://doi.org/10.1029/JZ066i001p00083>.
- Garfinkel, C. I., S. W. Son, K. Song, V. Aquila, and L. D. Oman, 2017: Stratospheric variability contributed to and sustained the recent hiatus in Eurasian winter warming. *Geophys. Res. Lett.*, **44**, 374–382, <https://doi.org/10.1002/2016GL072035>.
- , I. White, E. P. Gerber, S.-W. Son, and M. Jucker, 2021: Stationary wave and surface radiative effects weaken and delay the near-surface response to stratospheric ozone depletion. *Earth Space Sci. Open Archives*, 40 pp., <https://doi.org/10.1002/essoar.10508684.1>.
- Gerber, E. P., L. M. Polvani, and D. Ancukiewicz, 2008: Annular mode time scales in the intergovernmental panel on climate change fourth assessment report models. *Geophys. Res. Lett.*, **35**, L22707, <https://doi.org/10.1029/2008GL035712>.
- Gillett, N. P., T. D. Kell, and P. D. Jones, 2006: Regional climate impacts of the southern annular mode. *Geophys. Res. Lett.*, **33**, L23704, <https://doi.org/10.1029/2006GL027721>.
- Gnanadesikan, A., and Coauthors, 2006: GFDL's CM2 global coupled climate models. Part II: The baseline ocean simulation. *J. Climate*, **19**, 675–697, <https://doi.org/10.1175/JCLI3630.1>.
- Holton, J. R., and H.-C. Tan, 1980: The influence of the equatorial quasi-biennial oscillation on the global circulation at 50 mb. *J. Atmos. Sci.*, **37**, 2200–2208, [https://doi.org/10.1175/1520-0469\(1980\)037<2200:TIOTEQ>2.0.CO;2](https://doi.org/10.1175/1520-0469(1980)037<2200:TIOTEQ>2.0.CO;2).
- Horan, M. F., and T. Reichler, 2017: Modeling seasonal sudden stratospheric warming climatology based on polar vortex statistics. *J. Climate*, **30**, 10 101–10 116, <https://doi.org/10.1175/JCLI-D-17-0257.1>.
- Hoyer, S., and J. J. Hamman, 2017: xarray: N-D labeled arrays and datasets in Python. *J. Open Res. Software*, **5**, 10, <https://doi.org/10.5334/jors.148>.
- Hurwitz, M. M., P. A. Newman, L. D. Oman, and A. M. Molod, 2011: Response of the Antarctic stratosphere to two types of El Niño events. *J. Atmos. Sci.*, **68**, 812–822, <https://doi.org/10.1175/2011JAS3606.1>.
- , N. Calvo, C. I. Garfinkel, A. H. Butler, S. Ineson, C. Cagnazzo, E. Manzini, and C. Peña-Ortiz, 2014: Extra-tropical atmospheric response to ENSO in the CMIP5 models. *Climate Dyn.*, **43**, 3367–3376, <https://doi.org/10.1007/s00382-014-2110-z>.
- Jucker, M., 2016: Are sudden stratospheric warmings generic? Insights from an idealized GCM. *J. Atmos. Sci.*, **73**, 5061–5080, <https://doi.org/10.1175/JAS-D-15-0353.1>.
- , 2021a: aostools. Zenodo, <https://doi.org/10.5281/zenodo.597598>.
- , 2021b: Scaling of Eliassen-Palm flux vectors. *Atmos. Sci. Lett.*, **22**, e1020, <https://doi.org/10.1002/asl.1020>.
- , and T. Reichler, 2018: Dynamical precursors for statistical prediction of stratospheric sudden warming events. *Geophys. Res. Lett.*, **45**, 13 124–13 132, <https://doi.org/10.1029/2018GL080691>.
- , and R. Goyal, 2022: Ozone-forced southern annular mode during Antarctic stratospheric warming events. *Geophys. Res. Lett.*, **49**, e2021GL095270, <https://doi.org/10.1029/2021GL095270>.
- , T. Reichler, and D. W. Waugh, 2021: How frequent are Antarctic sudden stratospheric warmings in present and future climate? *Geophys. Res. Lett.*, **48**, e2021GL093215, <https://doi.org/10.1029/2021GL093215>.
- Kim, J., and T. Reichler, 2016: Quantifying the uncertainty of the annular mode time scale and the role of the stratosphere. *Climate Dyn.*, **47**, 637–649, <https://doi.org/10.1007/s00382-015-2860-2>.
- Kwon, H., H. Choi, B.-M. Kim, S.-W. Kim, and S.-J. Kim, 2020: Recent weakening of the southern stratospheric polar vortex and its impact on the surface climate over Antarctica.

- Environ. Res. Lett.*, **15**, 094072, <https://doi.org/10.1088/1748-9326/ab9d3d>.
- Lehtonen, I., and A. Y. Karpechko, 2016: Observed and modeled tropospheric cold anomalies associated with sudden stratospheric warmings. *J. Geophys. Res. Atmos.*, **121**, 1591–1610, <https://doi.org/10.1002/2015JD023860>.
- Lim, E.-P., H. H. Hendon, and D. W. Thompson, 2018: Seasonal evolution of stratosphere–troposphere coupling in the Southern Hemisphere and implications for the predictability of surface climate. *J. Geophys. Res. Atmos.*, **123**, 12 002–12 016, <https://doi.org/10.1029/2018JD029321>.
- , and Coauthors, 2021a: The 2019 Southern Hemisphere stratospheric polar vortex weakening and its impacts. *Bull. Amer. Meteor. Soc.*, **102**, E1150–E1171, <https://doi.org/10.1175/BAMS-D-20-0112.1>.
- , and Coauthors, 2021b: Tropical forcing of Australian extreme low minimum temperatures in September 2019. *Climate Dyn.*, **56**, 3625–3641, <https://doi.org/10.1007/s00382-021-05661-8>.
- Limpasuvan, V., D. W. Thompson, and D. L. Hartmann, 2004: The life cycle of the Northern Hemisphere sudden stratospheric warmings. *J. Climate*, **17**, 2584–2596, [https://doi.org/10.1175/1520-0442\(2004\)017<2584:TLCOTN>2.0.CO;2](https://doi.org/10.1175/1520-0442(2004)017<2584:TLCOTN>2.0.CO;2).
- Lin, P., Q. Fu, and D. L. Hartmann, 2012: Impact of tropical SST on stratospheric planetary waves in the Southern Hemisphere. *J. Climate*, **25**, 5030–5046, <https://doi.org/10.1175/JCLI-D-11-00378.1>.
- Newman, P. A., and E. R. Nash, 2005: The unusual Southern Hemisphere stratosphere winter of 2002. *J. Atmos. Sci.*, **62**, 614–628, <https://doi.org/10.1175/JAS-3323.1>.
- Plumb, R. A., and K. Semeniuk, 2003: Downward migration of extratropical zonal wind anomalies. *J. Geophys. Res.*, **108**, 4223, <https://doi.org/10.1029/2002JD002773>.
- Polvani, L. M., and D. W. Waugh, 2004: Upward wave activity flux as a precursor to extreme stratospheric events and subsequent anomalous surface weather regimes. *J. Climate*, **17**, 3548–3554, [https://doi.org/10.1175/1520-0442\(2004\)017<3548:UWAFAA>2.0.CO;2](https://doi.org/10.1175/1520-0442(2004)017<3548:UWAFAA>2.0.CO;2).
- Rao, J., C. I. Garfinkel, I. P. White, and C. Schwartz, 2020: The Southern Hemisphere minor sudden stratospheric warming in September 2019 and its predictions in S2S models. *J. Geophys. Res. Atmos.*, **125**, e2020JD032723, <https://doi.org/10.1029/2020JD032723>.
- Reichler, T., and J. Kim, 2008: How well do coupled models simulate today's climate? *Bull. Amer. Meteor. Soc.*, **89**, 303–312, <https://doi.org/10.1175/BAMS-89-3-303>.
- , and M. Jucker, 2022: Stratospheric wave driving events as an alternative to sudden stratospheric warmings. *Wea. Climate Dyn.*, **3**, 659–677, <https://doi.org/10.5194/wcd-3-659-2022>.
- , M. Dameris, and R. Sausen, 2003: Determining the tropopause height from gridded data. *Geophys. Res. Lett.*, **30**, 2042, <https://doi.org/10.1029/2003GL018240>.
- Roscoe, H. K., J. D. Shanklin, and S. R. Colwell, 2005: Has the Antarctic vortex split before 2002? *J. Atmos. Sci.*, **62**, 581–588, <https://doi.org/10.1175/JAS-3331.1>.
- Safieddine, S., and Coauthors, 2020: Antarctic ozone enhancement during the 2019 sudden stratospheric warming event. *Geophys. Res. Lett.*, **47**, e2020GL087810, <https://doi.org/10.1029/2020GL087810>.
- Saji, N., B. Goswami, P. Vinayachandran, and T. Yamagata, 1999: A dipole mode in the tropical Indian Ocean. *Nature*, **401**, 360–363, <https://doi.org/10.1038/43854>.
- Seviour, W. J. M., D. M. Mitchell, and L. J. Gray, 2013: A practical method to identify displaced and split stratospheric polar vortex events. *Geophys. Res. Lett.*, **40**, 5268–5273, <https://doi.org/10.1002/grl.50927>.
- Shen, X., L. Wang, and S. Osprey, 2020: Tropospheric forcing of the 2019 Antarctic sudden stratospheric warming. *Geophys. Res. Lett.*, **47**, e2020GL089343, <https://doi.org/10.1029/2020GL089343>.
- , —, —, S. C. Hardiman, A. A. Scaife, and J. Ma, 2022: The life cycle and variability of Antarctic weak polar vortex events. *J. Climate*, **35**, 2075–2092, <https://doi.org/10.1175/JCLI-D-21-0500.1>.
- Sjoberg, J. P., and T. Birner, 2012: Transient tropospheric forcing of sudden stratospheric warmings. *J. Atmos. Sci.*, **69**, 3420–3432, <https://doi.org/10.1175/JAS-D-11-0195.1>.
- Staten, P. W., and T. Reichler, 2014: On the ratio between shifts in the eddy-driven jet and the Hadley cell edge. *Climate Dyn.*, **42**, 1229–1242, <https://doi.org/10.1007/s00382-013-1905-7>.
- Stolarski, R. S., R. D. McPeters, and P. A. Newman, 2005: The ozone hole of 2002 as measured by TOMS. *J. Atmos. Sci.*, **62**, 716–720, <https://doi.org/10.1175/JAS-3338.1>.
- Thompson, D. W., M. P. Baldwin, and S. Solomon, 2005: Stratosphere–troposphere coupling in the Southern Hemisphere. *J. Atmos. Sci.*, **62**, 708–715, <https://doi.org/10.1175/JAS-3321.1>.
- Trenberth, K. E., and D. P. Stepaniak, 2001: Indices of El Niño evolution. *J. Climate*, **14**, 1697–1701, [https://doi.org/10.1175/1520-0442\(2001\)014<1697:LIOENO>2.0.CO;2](https://doi.org/10.1175/1520-0442(2001)014<1697:LIOENO>2.0.CO;2).
- Wang, L., S. C. Hardiman, P. E. Bett, R. E. Comer, C. Kent, and A. A. Scaife, 2020: What chance of a sudden stratospheric warming in the Southern Hemisphere? *Environ. Res. Lett.*, **15**, 104038, <https://doi.org/10.1088/1748-9326/aba8c1>.
- Wang, S., J. Liu, X. Cheng, T. Kerzenmacher, Y. Hu, F. Hui, and P. Braesicke, 2021: How do weakening of the stratospheric polar vortex in the Southern Hemisphere affect regional Antarctic sea ice extent? *Geophys. Res. Lett.*, **48**, e2021GL092582, <https://doi.org/10.1029/2021GL092582>.
- Wittenberg, A. T., A. Rosati, N.-C. Lau, J. J. Ploshay, A. T. Wittenberg, A. Rosati, N.-C. Lau, and J. J. Ploshay, 2006: GFDL's CM2 global coupled climate models. Part III: Tropical Pacific climate and ENSO. *J. Climate*, **19**, 698–722, <https://doi.org/10.1175/JCLI3631.1>.
- Yang, C., T. Li, X. Dou, and X. Xue, 2015: Signal of central Pacific El Niño in the Southern Hemispheric stratosphere during austral spring. *J. Geophys. Res. Atmos.*, **120**, 11 438–11 450, <https://doi.org/10.1002/2015JD023486>.